

Bachelor thesis

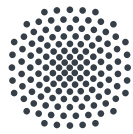
**Two-Photon spectroscopy of
rubidium in the vicinity of silicon
devices**

vorgelegt von

Wenting Chen

am 1. September 2019

Examiner: Prof. Dr. Tilman Pfau



University of Stuttgart
5th Institute of Physics

Contents

1	Introduction	3
2	Theory	5
2.1	Atom-Light-Interaction	5
2.2	Lineshape and broadening	8
2.2.1	Natural broadening	8
2.2.2	Doppler broadening	8
2.2.3	Transit-time broadening	9
2.2.4	Power broadening	10
3	D₂ line in Rubidium spectrum	13
3.1	Energy levels Structure	13
3.2	Calculation of Rabi frequency for hyperfine transitions	14
3.3	Calculation of branching ratio and decay rates of hyperfine levels	15
3.4	Comparison of MATLAB Simulation and Elecsus results	16
3.5	Saturation intensity	19
3.5.1	Faddeeva function for Voigt fitting	21
4	Two-photon spectroscopy	25
4.1	Excitation scheme and experimental Setup	25
4.1.1	Rabi frequency and saturation intensity of each transition	30
4.1.2	Calculation of branching ratio decay rates of hyperfine levels	30
4.1.3	Fitting results	31
4.2	Comparison between the experiment and the simulation	35
4.3	Polarization effect	36
5	Summary and Outlook	39
5.1	Time-dependent behaviour	39
5.2	Two-dimensional color map	45
	Bibliography	47

Ehrenwörtliche Erklärung

Ich erkläre,

- dass ich diese Bachelorarbeit selbständig verfasst habe,
- dass ich keine anderen als die angegebenen Quellen benutzt und alle wörtlich oder sinngemäß aus anderen Werken übernommenen Aussagen als solche gekennzeichnet habe,
- dass die eingereichte Arbeit weder vollsrändig noch in wesentlichen Teilen Gegenstand eines anderen Prüfungsverfahrens gewesen ist,
- dass ich die Arbeit weder vollständig noch in Teilen bereits veröffentlicht habe, es sei denn, der Prüfungsausschuss hat die Veröffentlichung vorher genehmigt,
- und dass der Inhalt des elektronischen Exemplars mit dem des Druckexemplars übereinstimmt.

Stuttgart, 30. August 2019

Wenting Chen

1 Introduction

Laser spectroscopy is a common technique for studying the properties of atoms. Energy levels, transition types, and their strengths can be investigated in the absorption spectrum.

The main purpose of this thesis is to simulate the two-photon spectra of $4D_{5/2}$ in Rubidium with a home-built MATLAB program and compare the results in a rubidium vapour cell with counter-propagating lasers, experimentally. This thesis begins with the fundamental theory used for the simulation. The main concept, i.e. optical Bloch equations, decay rate, line broadening are introduced. To simulate the interaction we construct a model by solving optical Bloch equations in MATLAB. The density matrix, which is relevant to the susceptibility calculation, is derived from these differential equations. For ^{85}Rb , we model a 12-level system involving $|5S_{1/2}\rangle$, $|5P_{3/2}\rangle$, $|4D_{5/2}\rangle$ hyperfine states. For ^{87}Rb , a 10-level system is constructed. As the input of the optical Bloch equations, all Rabi frequencies and decay rates are calculated. To consider the Doppler effect, the density matrix elements have been integrated for atoms with different velocities with Normal distributions. Using this integrated density matrix, the total induced dipole moment and susceptibility are calculated.

We first validate the results of our calculations for D2 with Elecsus, a software often used in atomic spectroscopy. Afterwards, we extend the study to two-photon case. A comparison between experimental spectrum and simulation spectrum, and a experiment with different laser polarization show the improvement space of our simulation. Finally, in the outlook chapter we present the time-dependent behaviour of the atom subject to two laser-beams. A two-dimensional map is included with varying detuning for both lasers.

2 Theory

The purpose of this chapter is to introduce a general method treating the atom-light-interaction by deriving the optical Bloch equations. From the solution of optical Bloch equations we get the the form of the density matrix, which plays a significant role in obtaining the absorption spectrum. Based on the theory presented in this chapter, we construct the model for the simulation in chapter 3 and 4.

2.1 Atom-Light-Interaction

Although a real atom is never a two-level system, it is sufficient to discuss the mechanism for atom-light-interaction by using a two-level system for presenting the main features. Afterwards, the principle obtaining the optical Bloch equations is applied to a 12-level system in ^{85}Rb and a 10-level system in ^{87}Rb .

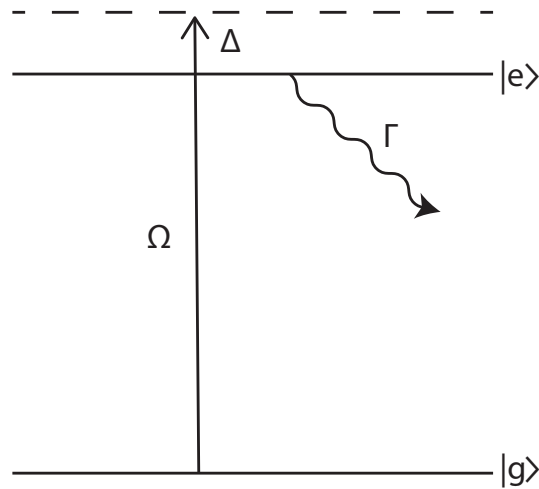


FIGURE 2.1: A two-level system with the ground state $|g\rangle$ and the excited state $|e\rangle$. In the figure Ω is the Rabi frequency and Γ is the population decay rate. The Detuning is defined as $\Delta = \omega_L - \omega_0$, where ω_L is the Laser frequency and ω_0 is the transition frequency.

A monochromatic light interacting with atom is presented as an electric field interacting with a dipole. Since the wavelength of the light is much longer than

the atomic size, it is fair to neglect the position dependent part

$$\mathbf{E}(t) = \mathbf{E}_0 \cdot \cos \omega t = \hat{\mathbf{e}} E_0 \cdot \frac{e^{-i\omega t} + e^{i\omega t}}{2} \quad (2.1)$$

where $\hat{\mathbf{e}}$ is the polarization unit-vector.

The total Hamiltonian for the system has two parts: 1) the free-atom part H_A corresponding to the eigen-energy for each state. 2) H_{AL} describing the interaction between the atom and electric field.

$$H = H_A + H_{AL} = \hbar\omega_0 |e\rangle\langle e| - \hat{\mathbf{d}} \cdot \mathbf{E} \quad (2.2)$$

$$= \hbar\omega_0 \sigma^\dagger \sigma - \langle g | \hat{\mathbf{d}} | e \rangle \cdot (\sigma + \sigma^\dagger) \cdot \hat{\mathbf{e}} \cdot E_0 / 2 \cdot (e^{i\omega t} + e^{-i\omega t}) \quad (2.3)$$

where $\hat{\mathbf{d}}$ is the dipole moment operator and $\sigma = |g\rangle\langle e|$ is the atomic lowering operator with the time dependence of $e^{-i\omega_0 t}$. The Hamiltonian in eq. (2.3) has two rapidly oscillating terms $e^{\pm i(\omega + \omega_0)t}$. These fast oscillating dynamics are negligible when the light frequency ω is near to the resonant frequency ω_0 . Therefore, a rotating-wave approximation (RWA) can be used to eliminate the fast oscillating terms and H_{AL} can be simplified as

$$H_{AL} = -\frac{1}{2} \cdot E_0 \cdot \langle g | \hat{\mathbf{e}} \cdot \mathbf{d} | e \rangle \cdot (\sigma e^{i\omega t} + \sigma^\dagger e^{-i\omega t}) \quad (2.4)$$

$$= \frac{\hbar\Omega}{2} \cdot (\sigma e^{i\omega t} + \sigma^\dagger e^{-i\omega t}) \quad (2.5)$$

where the Rabi frequency is defined as

$$\Omega = -\frac{\langle g | \hat{\mathbf{e}} \cdot \mathbf{d} | e \rangle \cdot E_0}{\hbar} \quad (2.6)$$

The atom-light interacting Hamiltonian of eq. (2.5) is still time-dependent. A unitary transformation in the form of $U = e^{i\omega t} |e\rangle\langle e|$ helps to remove the explicit time dependency and leads to a more efficient transformed Hamiltonian for the calculation. The rotated Hamiltonian read as

$$\tilde{H} = U H U^\dagger + i\hbar \frac{\partial U}{\partial t} \cdot U^\dagger \quad (2.7)$$

Using the eq. (2.7) in (2.5), the total Hamiltonian is given by

$$\tilde{H} = \tilde{H}_A + \tilde{H}_{AL} = -\hbar \cdot \Delta |e\rangle\langle e| + \frac{\hbar\Omega}{2} (\sigma + \sigma^\dagger) \quad (2.8)$$

where Δ is the detuning $\omega - \omega_0$.

A density matrix represents the state of a mixed quantum system. The trace of this matrix is one. The diagonal entries represent the population at each energy level, while the non-diagonal entries correspond to the coherence between two states. The quantum mechanical expectation value of any observable, e.g. the dipole moment, is given by the trace of the product of the density matrix and that operator, as

$$\langle \hat{O} \rangle = \text{tr}(\hat{\rho} \cdot \hat{O}) \quad (2.9)$$

where O depicts the observable. The master equations (2.10) is differential equation that relates the density matrix and its derivatives. For an open quantum system, the consideration of decay and phase decoherence are necessary. The Lindblad superoperator captures all the dissipations (sum of all m decay channels) of energy into surroundings.

$$\frac{\partial \tilde{\rho}(t)}{\partial t} = -\frac{i}{\hbar} \left[\hat{H}(t), \tilde{\rho}(t) \right] + \tilde{L}(\tilde{\rho}) \quad (2.10)$$

whereas $\tilde{L}(\tilde{\rho})$ is given by:

$$\tilde{L}(\tilde{\rho}) = \sum_m \Gamma_m \cdot (a_m \tilde{\rho} a_m^\dagger - \frac{1}{2} \cdot (a_m^\dagger a_m \tilde{\rho} + \tilde{\rho} a_m^\dagger a_m)) \quad (2.11)$$

where a_m is an arbitrary operator and $\tilde{\rho}$ is the density matrix. In the matrix form it should follow the rule that all states' populations sum up to 1, which means $\sum_{i=1}^n \langle i | \tilde{\rho} | i \rangle$ with n as the total number of states.

Based on the master equation, we could derive the optical Bloch equation for a two-level system [1].

$$\frac{\partial \tilde{\rho}_{gg}}{\partial t} = \Gamma_0 \tilde{\rho}_{ee} - \text{Im}(\Omega_0^* \tilde{\rho}_{ge}) \quad (2.12)$$

$$\frac{\partial \tilde{\rho}_{ge}}{\partial t} = -(\Gamma_0/2 + i\Delta) \tilde{\rho}_{ge} - i\Omega_0/2 (\tilde{\rho}_{ee} - \tilde{\rho}_{gg}) \quad (2.13)$$

$$\frac{\partial \tilde{\rho}_{eg}}{\partial t} = (i\Delta - \Gamma_0/2) \tilde{\rho}_{eg} + i\Omega_0/2 (\tilde{\rho}_{ee} - \tilde{\rho}_{gg}) = \frac{\partial \tilde{\rho}_{ge}^*}{\partial t} \quad (2.14)$$

$$\frac{\partial \tilde{\rho}_{ee}}{\partial t} = -\Gamma_0 \tilde{\rho}_{ee} + \text{Im}(\Omega_0^* \tilde{\rho}_{ge}) = -\frac{\partial \tilde{\rho}_{gg}}{\partial t} \quad (2.15)$$

The solution of the optical Bloch equations for $\tilde{\rho}$ is a time-dependent density matrix. To obtain the density matrix at steady state, the left part of the optical Bloch equations (2.12) to (2.15) should be zero.

2.2 Lineshape and broadening

The absorption lines of any real emitter has a finite width. In general, the line shape is both homogeneously and inhomogeneously broadened. In this part we introduce four main types of broadening, natural broadening, Doppler broadening, transit-time broadening, and power broadening. The collisional broadening is negligible in the experiment due to the low density in the vapour cell [2].

2.2.1 Natural broadening

The spontaneous emission in the excited states is responsible for the natural broadening. The coupling of the atom to the electromagnetic vacuum field results in the decay to the ground state and the photon emission. Due to this probability event, an excited atom does not stay in the excited level but has a finite lifetime τ , which is the inverse of the decay rate Γ . According to Heisenberg's uncertainty principle, the energy of each quantum state has an uncertainty

$$\Delta E \geq \frac{\hbar}{\Delta t} \quad (2.16)$$

For atoms, the time uncertainty Δt in the eq. (2.16) is equals to the lifetime τ . The exponentially decaying behavior in time results in Lorentz shape in the frequency spectrum [2].

2.2.2 Doppler broadening

The random thermal motion of atoms leads to a Boltzmann distribution of atomic velocity. A moving atom sees an altered frequency of light due to the Doppler effect. The frequency difference can be written in product of wave-vector \mathbf{k} and velocity \mathbf{v}

$$\omega' = \omega - \mathbf{k} \cdot \mathbf{v} \quad (2.17)$$

This frequency shift results in a shifted detuning as

$$\Delta = \Delta - \mathbf{k} \cdot \mathbf{v} \quad (2.18)$$

The contribution of Doppler broadening on a Lorentz line shape leads to a Voigt profile:

$$V(\omega) = \frac{a}{\sqrt{2\pi}\sigma} \int_{-\infty}^{\infty} \frac{\exp\left\{-\frac{v^2}{2\sigma^2}\right\}}{(\omega - \omega_0 - \mathbf{k} \cdot \mathbf{v})^2 + (\Gamma_L/2)^2} dv$$

where a is the amplitude involving the vapour density and Lorentz width Γ_L . For Voigt profile, the FWHM of Voigt (Γ_V) is built up by FWHM of Doppler (Γ_D) and FWHM of Lorentz (Γ_L). With approximation it can be written as [3]:

$$\Gamma_V = 0.5346\Gamma_L + \sqrt{0.2166\Gamma_L^2 + \Gamma_D^2} \quad (2.19)$$

2.2.3 Transit-time broadening

If the cross-section of a laser beam is small, the interaction time of atoms with field can be smaller than the spontaneous lifetime. Hence, the time uncertainty in eq. (2.16) is no longer the lifetime of atom but the interaction time. This leads to the transit-time broadening of the lineshape. The transit rate is defined as $\Gamma_t = \bar{v}/\bar{d}$, where \bar{v} is the average atomic speed and \bar{d} is the average path length across the beam cross-section. We assume that the atomic velocity has a Boltzmann distribution and the beam profile has a circular shape, therefore we get $\bar{v} = \sqrt{\frac{\pi k_B T}{2m}}$ and $\bar{d} = \frac{\pi D}{4}$ with D as the beam diameter. The transit rate is given by [4]

$$\Gamma_t = \frac{\sqrt{8k_B T/\pi m}}{D} \approx 1.13 \cdot \frac{\sigma}{D} \quad (2.20)$$

where $\sigma = \sqrt{2k_B T/m}$ is the two dimensional root-mean-squared velocity.

In our experiment, the beam cross-section is large enough for an atom to interact with the light within its lifetime and before it leaves the beam area. The transit-time effect on the line-width is negligible. However, it is necessary to introduce a transit rate between $|5S_{1/2}, F = 2\rangle$ and $|5S_{1/2}, F = 3\rangle$ (the ground hyperfine states) in order to prevent all atoms going to the dark state $|5S_{1/2}, F = 2\rangle$ at long times. Two ground states $|5S_{1/2}, F = 2\rangle$ and $|5S_{1/2}, F = 3\rangle$ are separated by 3 GHz. Since the 780 nm laser is locked to the transition $|5S_{1/2}, F = 3\rangle \rightarrow |5P_{3/2}, F' = 4\rangle$, the atoms excited from $F = 3$ to $|5P_{3/2}, F' = 2, 3\rangle$ and then decaying to $|5S_{1/2}, F = 2\rangle$ are not able to be excited back to the $5P_{3/2}$. Therefore, atoms staying long-enough inside the beam would go to $|5S_{1/2}, F = 2\rangle$ and stay there, hence pumped to the dark state.

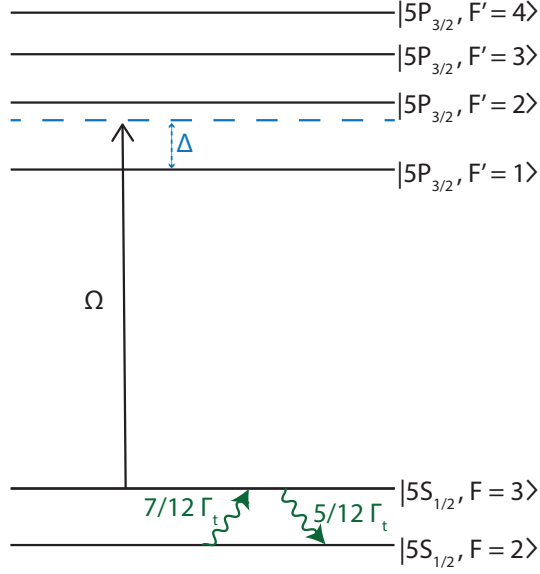


FIGURE 2.2: The transit relation effect between two $5S_{1/2}$ states are shown in green wavy line. The Rabi frequency is Ω and the detuning is Δ .

The transit rate for hyperfine ground state is distributed according to the degeneracy of the levels [4]

$$\Gamma_{F=2 \rightarrow F=3} = \frac{7}{12} \cdot \Gamma_t$$

$$\Gamma_{F=3 \rightarrow F=2} = \frac{5}{12} \cdot \Gamma_t$$

For simulation, by introducing the transit rate into the decay rate matrix, we obtain a pseudo steady-state model to calculate the atomic density matrix. The model assumes that there is a cut-point before the system goes to the real steady state. At that point all the levels are properly included.

2.2.4 Power broadening

The spectral width increases when the intensity of the laser increases. It is known as power broadening, a homogeneous broadening in spectroscopy.

At low intensity, the commutator of lowering operator $[\sigma, \sigma^\dagger] = |g\rangle\langle g| - |e\rangle\langle e| \approx 1$, since there are few atoms in the excited state. Therefore, we could regard the atom as a harmonic oscillator with this assumption the Lorentz linewidth of spectrum approaches to the natural line width Γ at low intensity [2].

At higher intensities, more atoms are pumped to the excited state, correspondingly more decaying towards the opposite direction happens. These two contrary processes

lead to an increased Lorentz width, a phenomenon known as saturation.

It is sufficient to use a two-level system, as the fig. (2.1) shows. From the master equation for two level system at steady-state, the population difference between the ground and the excited state is given by

$$(\rho_{ee} - \rho_{gg})_{ss} = \frac{-1}{1 + \frac{\gamma/\Gamma}{\gamma^2 + \Delta^2} \Omega^2} = \frac{-1}{1 + \frac{\Omega^2 L(\Delta)}{\gamma\Gamma}} \quad (2.21)$$

with a Lorentz lineshape defined as

$$L(\Delta) = \frac{\gamma^2}{\gamma^2 + \Delta^2} \quad (2.22)$$

The electric field of plane wave is $E = \sqrt{2I/\epsilon_0 c}$. Therefore, the Rabi frequency can be replaced by the intensity with prefactor

$$\Omega^2 = \frac{d^2 E^2}{\hbar^2} = \frac{d^2 2c\mu_0 I}{\hbar^2} \quad (2.23)$$

where d is the transition dipole moment. Eq. (2.21) can be written as

$$(\rho_{ee} - \rho_{gg})_{ss} = \frac{-1}{1 + \frac{I}{I_{\text{sat}}} L(\Delta)} \quad (2.24)$$

In a low density vapour the collisions between atoms are negligible. In this case only the natural decoherence exists and the decoherence rate $\gamma = \Gamma/2$ and the saturation intensity is given by

$$I_{\text{sat}} = \frac{\epsilon_0 c \hbar^2 \Gamma^2}{4d^2} \quad (2.25)$$

The master equation also gives the induced dipole moment at steady state

$$d = -i \frac{\Omega}{2} \frac{\rho_{ss} - \rho_{gg}}{\gamma + i\Delta} = \frac{\Omega}{2} \frac{L(\Delta)}{1 + \frac{I}{I_{\text{sat}}} L(\Delta)} \times \frac{\gamma - i\Delta}{\gamma^2}, \quad (2.26)$$

The absorption of the signal α is the imaginary part of induced dipole moment

$$\alpha = \frac{\Omega}{2\gamma} \frac{L(\Delta)}{1 + \frac{I}{I_{\text{sat}}} L(\Delta)} \quad (2.27)$$

For low intensity case, i.e. $I \ll I_{\text{sat}}$, the absorption approaches $\frac{\Gamma}{2\gamma} L(\Delta)$ with Lorentz lineshape and leads to $\Gamma_L = \Gamma$.

When the intensity is much larger than I_{sat} , the equation (2.27) turns to

$$\alpha = \frac{\Omega\gamma/2}{\Delta^2 + \gamma^2(1 + \frac{I}{I_{\text{sat}}})} \quad (2.28)$$

This leads to the function for FWHM of Lorentz lineshape

$$\Gamma_L = \Gamma_0 \sqrt{1 + \frac{I}{I_{\text{sat}}}} \quad (2.29)$$

In experiments, sometimes the background offset should also be considered, e.g. the line broadening due to the magnetic field. We put a general offset Γ_{off} to the eq. (2.29)

$$\Gamma_L = \Gamma_0 \sqrt{1 + \frac{I}{I_{\text{sat}}}} + \Gamma_{\text{off}} \quad (2.30)$$

3 D₂ line in Rubidium spectrum

In this thesis, the D₂ line refers to the transition $|5S_{1/2}\rangle \rightarrow |5P_{3/2}\rangle$ in Rubidium spectroscopy. The hyperfine structure of ^{87}Rb and ^{85}Rb for this D₂ line involves six energy levels. In this chapter we compare the D₂ line at low intensity from the MATLAB simulation with the Elecsus software. Afterwards, the simulated spectra as various powers are fitted to determine the Lorentz widths. The Lorentz widths following the power broadening relation help us to get the saturation intensity and compare it with the theoretical value calculated from transition features.

3.1 Energy levels Structure

This section involves the transition $|5S_{1/2}\rangle \rightarrow |5P_{3/2}\rangle$ (D₂-line) of Rubidium. The hyperfine structure is considered here, which includes the energy splitting due to the coupling of total electron angular momentum \mathbf{J} with the total nuclear angular momentum \mathbf{I} . The ground state $|5S_{1/2}\rangle$ splits to 2 sub-levels and the excited state $|5P_{3/2}\rangle$ splits to 4 sub-levels. The 780 nm laser is scanned over this transition and pumps the atom to the upper level. Meanwhile an atom at the excited state decays to the ground state with the decay rate of $2\pi \cdot 6.066$ MHz [5].

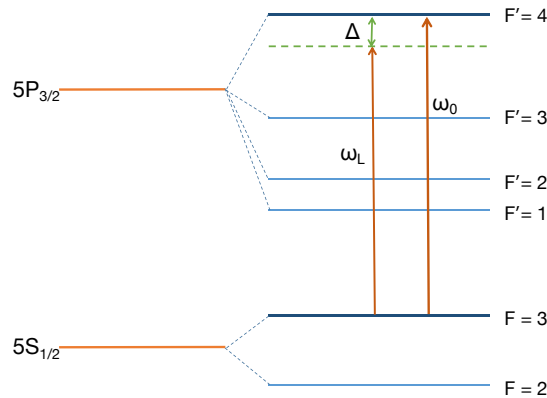


FIGURE 3.1: Rubidium 85 energy level scheme for the excitation from the ground state $|5S_{1/2}\rangle$ to the excited state $|5P_{3/2}\rangle$. ω_L is the laser frequency and Δ indicates the detuning. The cyclic transition is $|5S_{1/2}, F=3\rangle \rightarrow |5P_{3/2}, F=4\rangle$. The energy gap between those two levels is $\hbar\omega_0$.

3.2 Calculation of Rabi frequency for hyperfine transitions

The Rabi frequency Ω_q is defined in chapter 2 as:

$$\Omega_q = -\frac{\langle g|\hat{\epsilon} \cdot \mathbf{d}|e\rangle E_q}{\hbar} \quad (3.1)$$

whereas $\hat{\epsilon}$ is the polarisation operator and E_q is the exciting electric field. In our simulation, the Rabi frequency for each hyperfine transition is needed, and in this case the ground state $|g\rangle$ is $|5S_{1/2}, F\rangle$ and the excited state $|e\rangle$ is $|5P_{3/2}, F'\rangle$. The whole induced dipole moment including all S to P transitions is the sum of dipole moments from all hyperfine sublevels. Considering the symmetry of dipole operator, we use the factor $S_{FF'}$ to exhibit the relative strength of dipole moment of each $|F\rangle \rightarrow |F'\rangle$ transition [5, 6].

$$S_{FF'} = \sum_q (2F' + 1)(2J + 1) \left\{ \begin{matrix} J & J' & 1 \\ F' & F & I \end{matrix} \right\}^2 |\langle Fm_F|F' 1 (m_F - q)q\rangle|^2 \quad (3.2)$$

$$= (2F' + 1)(2J + 1) \left\{ \begin{matrix} J & J' & 1 \\ F' & F & I \end{matrix} \right\}^2 \quad (3.3)$$

where F is the total atomic angular momentum quantum number, J is the quantum number of the total electron angular momentum, I is the nuclear angular momentum quantum number. The curly brackets denote the Wigner 6-j symbol. The primed letters indicate excited state levels. In an isotropic pump field, the strength of each polarisation takes up one third of $S_{FF'}$, as only one third of the dipole moment would be induced by the given polarization of the field. Therefore, the Rabi frequency is given by

$$\Omega_{\text{isotropic}} = \frac{\sqrt{\frac{S_{FF'}}{3}} \cdot |\langle J||\hat{\epsilon}\mathbf{d}||J'\rangle| \cdot E}{\hbar} \quad (3.4)$$

$$(3.5)$$

The reduced dipole moment magnitude $|\langle J||\hat{\epsilon}\mathbf{d}||J'\rangle|$ is given by the eq (3.9).

Another way to calculate the hyperfine transition strength for the Rabi frequency is to sum all transition strengths of Zeeman sublevels in a hyperfine manifold up. A prefactor calculating different Rabi frequencies in hyperfine structure for a certain transition q is defined as C_q .

$$\Omega_q = \frac{\sqrt{C_q} \cdot |\langle J||\hat{\epsilon}\mathbf{d}||J'\rangle| \cdot E}{\hbar} \quad (3.6)$$

Ω_q corresponds to the Rabi frequency for certain polarisation π, σ^+, σ^- . C_q is proportional to the total strength factor $C_{F,F'}^2$, which sums all transition strengths of each Zeeman transition $C_{m_F, m_{F'}}^2$ up [7].

$$C_q = \frac{C_{F,F'}^2}{2F+1} = \frac{\sum C_{m_F, m_{F'}}^2}{2F+1} \quad (3.7)$$

$2F+1$ denotes the degeneracy of the ground state. The transition prefactor $C_{m_F, m_{F'}}$ indicates multiples of the $\langle J || e\mathbf{r} || J' \rangle$ in the dipole matrix element $\langle F, m_F | e\mathbf{r}_q | F', m_{F'} \rangle$, which couples two Zeeman sublevels.

$$\langle F, m_F | e\mathbf{r}_q | F', m_{F'} \rangle = C_{m_F, m_{F'}} \cdot \langle J || e\mathbf{r}_q || J' \rangle \quad (3.8)$$

Table (3.1) gives these coefficients for each transition in hyperfine structure. As expected, the calculation using $S_{FF'}$ and $C_{m_F, m_{F'}}$ lead to the same results.

$^{85}\text{Rb}(5S_{1/2} \rightarrow 5P_{3/2})$			$^{87}\text{Rb}(5S_{1/2} \rightarrow 5P_{3/2})$		
$5S_{1/2}, F \rightarrow 5P_{3/2, F'}$	$S_{FF'}/3$	C_q	$5S_{1/2}, F \rightarrow 5P_{3/2, F'}$	$S_{FF'}/3$	C_q
$(F=2 \rightarrow F'=1)$	1/10	0.1	$(F=1 \rightarrow F'=0)$	1/18	0.0556
$(F=2 \rightarrow F'=2)$	7/54	0.1296	$(F=1 \rightarrow F'=1)$	5/36	0.1389
$(F=2 \rightarrow F'=3)$	14/135	0.1037	$(F=1 \rightarrow F'=2)$	5/36	0.1389
$(F=3 \rightarrow F'=2)$	5/189	0.0265	$(F=2 \rightarrow F'=1)$	1/60	0.0167
$(F=3 \rightarrow F'=3)$	5/54	0.0926	$(F=2 \rightarrow F'=2)$	1/12	0.0833
$(F=3 \rightarrow F'=4)$	3/14	0.2143	$(F=2 \rightarrow F'=3)$	7/30	0.2333

TABLE 3.1: Dipole moment prefactor for hyperfine transitions of $5S_{1/2} \rightarrow 5P_{3/2}$ (D₂-line for both rubidium isotopes)

3.3 Calculation of branching ratio and decay rates of hyperfine levels

The spontaneous decay rate, i.e. the inverse of lifetime, for each $J \rightarrow J'$ transition, can be calculated by reduced dipole moment and the resonant frequency [5].

$$\Gamma(J, J') = \frac{1}{\tau} = \frac{\omega^3}{3\pi\epsilon_0\hbar c^3} \frac{2J+1}{2J'+1} |\langle J || e\mathbf{r} || J' \rangle|^2 \quad (3.9)$$

where ω is the transition frequency between the fine structure.

If the energy level can decay to more than one level in the ground state, the branching ratio for each possible decay path should be taken into account. For

example, ⁸⁵Rb atoms at $|5P_{3/2}, F' = 3\rangle$ decay to the state $|5S_{1/2}, F = 2\rangle$ with the decay rate $\Gamma_{2,3}$ or $|5S_{1/2}, F = 3\rangle$ with the decay rate $\Gamma_{3,3}$. The branching ratio $B_{F,F'}$ for the first transition is $B_{2,3} = \frac{\Gamma_{2,3}}{\Gamma(J=\frac{1}{2}, J'=\frac{3}{2})}$. The ratio is the sum of $C_{m_F, m_{F'}}^2$ divided by F' -degeneracy of upper state and multiplied by a prefactor $\frac{2J'+1}{2J+1}$ [8]

$$B_{F,F'} = \frac{2J' + 1}{2J + 1} \cdot \sum_q C_{m_F, m_{F'}}^2 \cdot \frac{1}{2F' + 1} \quad (3.10)$$

$$\Gamma_{F,F'} = B_{F,F'} \cdot \Gamma(J, J') \quad (3.11)$$

More specifically, the decay rate can be written in the form of

$$\Gamma_{F,F'} = \frac{\omega^2}{3\pi\epsilon_0\hbar c^3} \cdot (2F + 1)(2J + 1) \cdot \left\{ \begin{matrix} J & J' & 1 \\ F' & F & I \end{matrix} \right\}^2 \cdot |\langle J || \mathbf{er} || J' \rangle|^2 \quad (3.12)$$

Transition	$B_{FF'}$ of ⁸⁵ Rb	Transition	$B_{FF'}$ of ⁸⁷ Rb
$(F = 2 \rightarrow F' = 1)$	1	$(F = 1 \rightarrow F' = 0)$	1
$(F = 2 \rightarrow F' = 2)$	0.8333	$(F = 1 \rightarrow F' = 1)$	0.8333
$(F = 2 \rightarrow F' = 3)$	0.1667	$(F = 1 \rightarrow F' = 2)$	0.1667
$(F = 3 \rightarrow F' = 2)$	0.5	$(F = 2 \rightarrow F' = 1)$	0.5
$(F = 3 \rightarrow F' = 3)$	0.5	$(F = 2 \rightarrow F' = 2)$	0.5
$(F = 3 \rightarrow F' = 4)$	1	$(F = 2 \rightarrow F' = 3)$	1

TABLE 3.2: Branching ratios for hyperfine transitions of $5S_{1/2} \rightarrow 5P_{3/2}$ (D₂-line for both rubidium isotopes)

3.4 Comparison of MATLAB Simulation and Elecsus results

In order to test the validity of the Simulation model, we compare the produced results from the MATLAB simulation with Elecsus results. Elecsus is a programme that calculates the susceptibility by adding the contributions of all transitions modeled as Lorentzian lineshapes [9]. It is used for the weak-probe regime and has an excellent agreement with experimental data. Hence, it is used as a reference for our simulation. Fig. (3.2) to (3.4) show the comparison of our simulation results with Elecsus at temperature =20°.

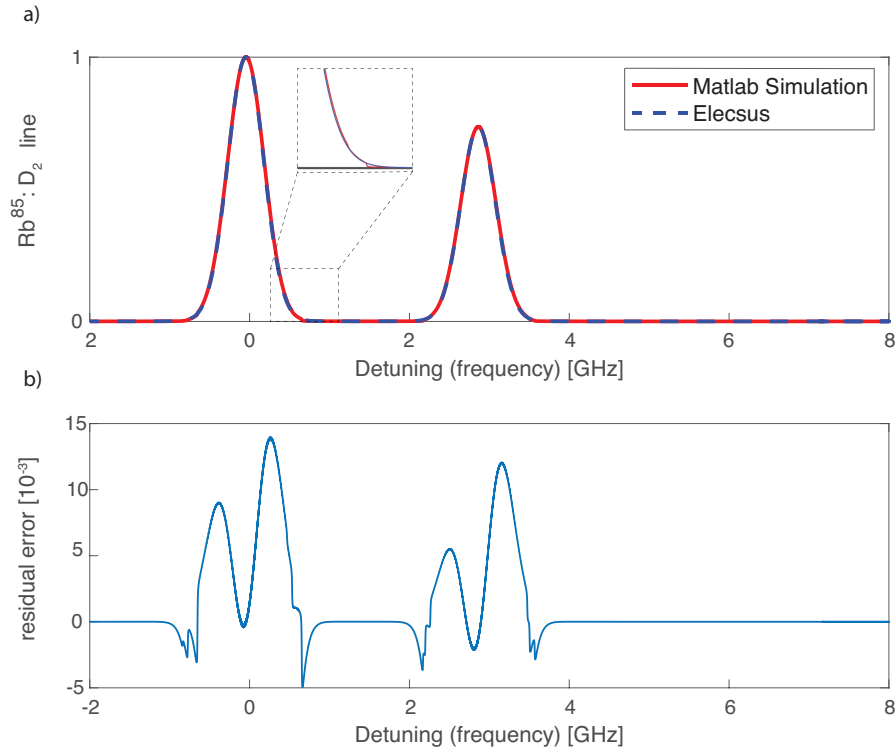


FIGURE 3.2: Comparison between MATLAB Simulation of ^{85}Rb at low intensity $I = 10^{-10}$ mW/cm^2 and Elecsus result at temperature $=20^\circ$. Zero detuning corresponds to the cyclic transition $|5S_{1/2}F = 3\rangle \rightarrow |5P_{3/2}F = 4\rangle$. Panel a) shows the normalized induced dipole moment spectrum. Panel b) shows the error between two spectra defined as $S_{\text{matlab}} - S_{\text{elecsus}}$ (S means signal). The inset in panel (a) shows the difference between two signals. This difference results from the atomic velocity sampling in MATLAB simulation. The maximum velocity used in our calculations is 4σ . If we increase the sampling range to 5σ or more for the Matlab calculation, where $\sigma = \sqrt{k_B T / m_{\text{Rb}}}$ is the standard deviation of one-dimensional velocity, the simulation signal will be smoother and the error will decrease.

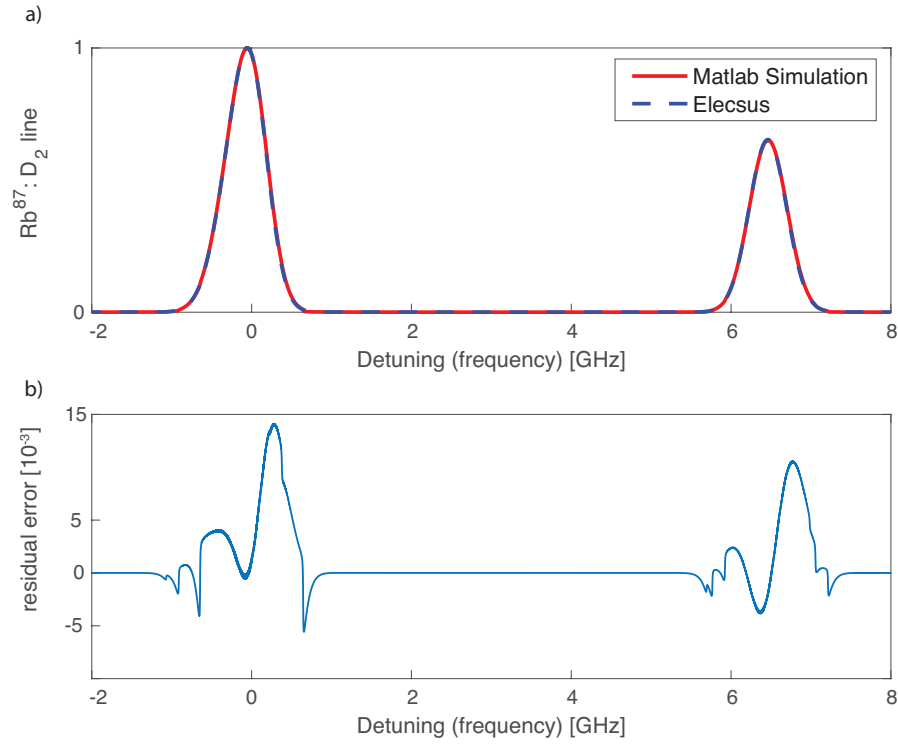


FIGURE 3.3: Comparison between MATLAB Simulation of ⁸⁷Rb at low intensity $I = 10^{-10}$ mW/cm² and Elecsus result. Peak at zero Detuning indicates the cyclic transition $5S_{1/2}, F = 2 \rightarrow |5P_{3/2}, F = 3\rangle$

Fig (3.4) shows the whole Rubidium D₂ spectrum, including ⁸⁵Rb and ⁸⁷Rb with the natural abundance $NA_{85} = 72.17\%$, $NA_{87} = 27.83\%$ [5]. This complete spectrum is produced by

$$d_{\text{total}} = NA_{85} \cdot d_{s^{85}\text{Rb}} + NA_{87} \cdot d_{s^{87}\text{Rb}}$$

where d_{total} is the total induced dipole moment. $d_{s^{85}\text{Rb}}$ and $d_{s^{87}\text{Rb}}$ are individual induced dipole moment of isotope, generated by 12-level and 10-level MATLAB simulation respectively.

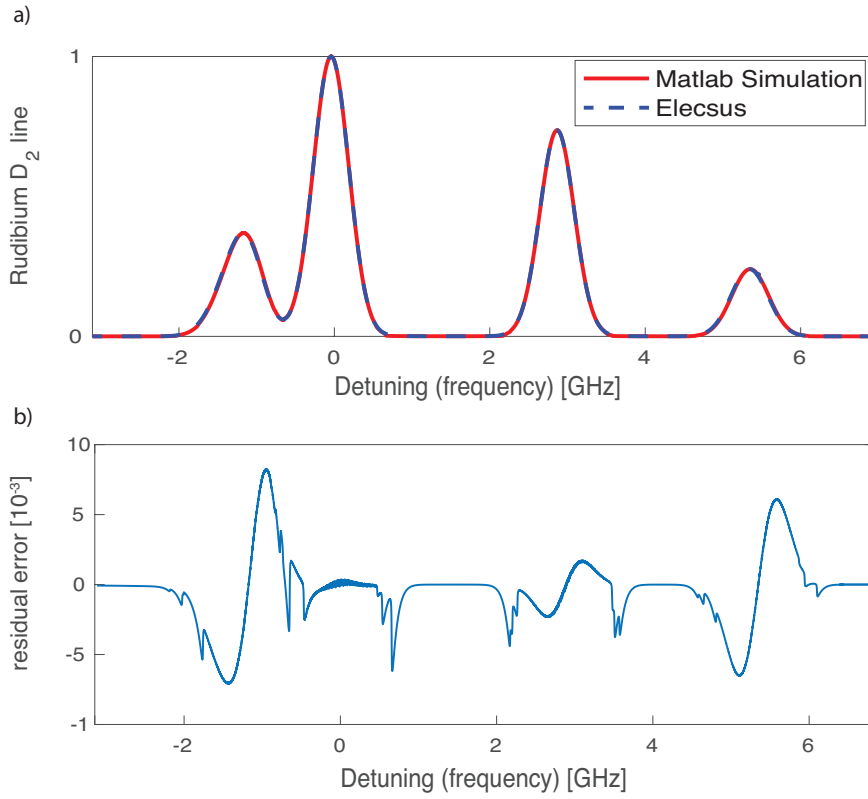


FIGURE 3.4: Comparison between MATLAB Simulation of the whole Rb spectrum at low intensity $I = 10^{-10}$ mW/cm² and Elecsus result at temperature=20°. Zero detuning corresponds to the cyclic transition $|5S_{1/2}, F = 2\rangle \rightarrow |5P_{3/2}, F = 3\rangle$.

From this comparison we can see that the simulation for low power matches well with Elecsus result.

3.5 Saturation intensity

As mentioned in the chapter 2, by increasing the intensity of either 780 nm or 1529 nm light, we are able to see that the power broadening has an effect on strength for different transition. In theory, the saturation intensity can be calculated by natural linewidth(decay rate) Γ and induced dipole moment $\hat{e} \cdot d$.

$$I_{\text{sat}} = \frac{c\epsilon_0\Gamma^2\hbar^2}{4|\hat{e} \cdot d|} \quad (3.13)$$

where ϵ_0 is the vacuum permittivity and c is the light speed.

For ⁸⁵Rb D₂ line, we use the dipole moment of the cyclic transition $|5S_{1/2}, F = 3\rangle \rightarrow |5P_{3/2}, F = 4\rangle$, the largest induced dipole moment $|\hat{e} \cdot d| = 1.9575 e a_0$ among

all six transitions in $5S_{1/2}$ to $5P_{3/2}$ excitation, to calculate the total saturation intensity for $5S_{1/2}$ to $5P_{3/2}$ transition. The $I_{\text{sat},85}$ is 3.895 mW/cm^2 . Similarly, the saturation intensity of ^{87}Rb $I_{\text{sat},87}$ is 3.576 mW/cm^2 .

At first we set the atomic velocity at zero in MATLAB simulation to simulate a still atom. As a result, a spectrum including 12 peaks is obtained. The sixth peak corresponds to the cyclic transition of ^{85}Rb ($|5S_{1/2}, F = 3\rangle \rightarrow |5P_{3/2}, F' = 4\rangle$).

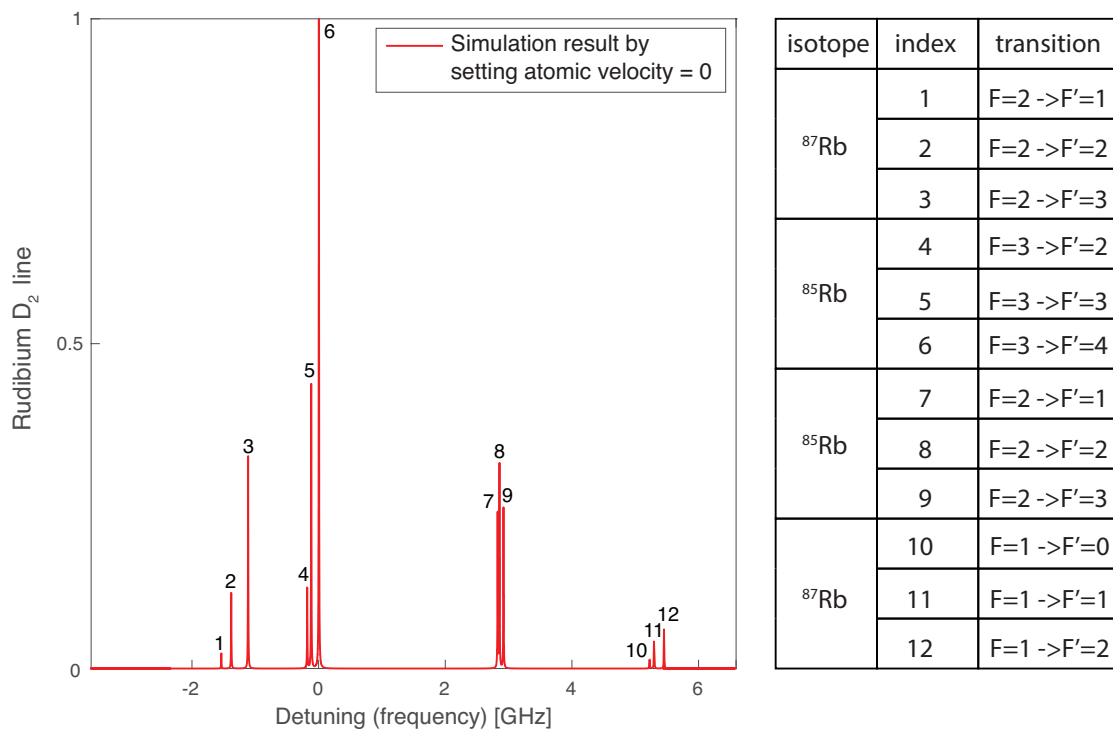


FIGURE 3.5: Simulation result of Rubidium D₂ line for a still atom. The peak's index and its corresponding transition $|5S_{1/2}, F\rangle \rightarrow |5P_{1/2}, F'\rangle$ are presented in the table on the right side.

According to the theory of Doppler broadening in chapter 2, if the atomic velocity is changed to another value v , the spectrum would receive a shift kv along the x-axis. The entire spectrum including all velocities in Gaussian distribution can be seen as a superposition of all simple-velocity spectra. When the 780 nm laser intensity increases, the Lorentz widths of each transition increase following the eq. (2.29). As the saturation intensities are different according to the eq. (3.13), eq. (3.8) and table (3.1), the Lorentz widths rise differently.

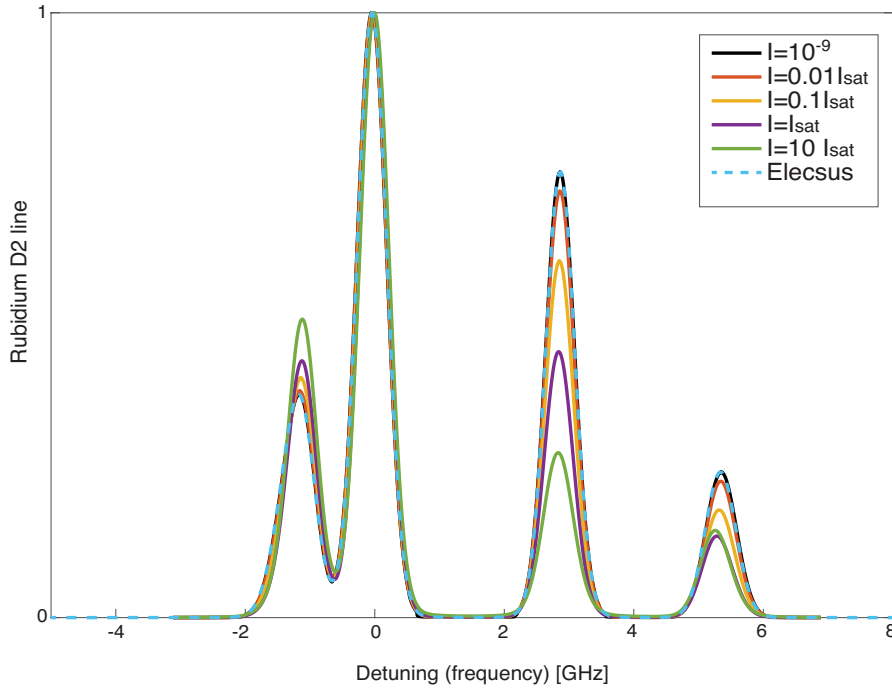


FIGURE 3.6: Normalized Rubidium D₂ line produced by MATLAB simulation for different 780 nm intensities.

By analysing the Voigt profile, it is able to get the Lorentz full width at half maximum (FWHM) at different intensity and then calculate the saturation intensity.

$$\Gamma = \Gamma_0 \cdot \sqrt{1 + \frac{I}{I_{\text{sat}}}} \quad (3.14)$$

3.5.1 Faddeeva function for Voigt fitting

Faddeeva function is a complex complementary error function [10]. The real part of Voigt fitting has the form of Faddeeva function. In the profile fitting we use this error function to separate the Doppler broadening and Lorentz linewidth of the profile. the Voigt profile can be regard as a Doppler broadened Lorentz profile and given by

$$V(f) = \frac{a}{\sqrt{2\pi}\sigma} \int_{-\infty}^{\infty} \frac{\exp\left\{-\frac{v^2}{2\sigma^2}\right\}}{(f - f_0 - k \cdot v)^2 + (\Gamma/2)^2} dv$$

where k is the wavenumber of laser, f is the frequency, σ is the standard deviation of Gaussian distribution and Γ is the Lorentz FWHM. For the transition $5S_{1/2}$ to $5P_{3/2}$,

the wavenumber $k = 2\pi/\lambda =$ With substitution $r = \frac{v}{\sqrt{2}\sigma}$, $x = \frac{f-f_0}{\sqrt{2}\sigma k}$, $y = \frac{\Gamma}{2k\sqrt{2}\sigma}$

$$V(x) = \frac{a \cdot \sqrt{2\pi}}{\sigma k \Gamma} \cdot \int_{-\infty}^{\infty} \frac{y \exp\{-r^2\}}{\pi (x-r)^2 + y^2} dr$$

$$= s \cdot \text{Re}[\text{Fadf}(x + i \cdot y)]$$

$$\text{Fadf}(z) = \frac{i}{\pi} \int_{-\infty}^{\infty} \frac{\exp\{-t^2\}}{z-t} dt, \quad z = x + iy \text{ is a complex number}$$

In total, there are 14 parameter to be fitted. They are 12 peaks' height, the Doppler width and the Lorentz width. Therefore a proper initial guess takes an important role in the fitting process. The Gaussian standard deviation is a constant that only depends on the temperature and Rubidium mass. After fixing peaks positions, i.e. resonance frequencies, an initial strength guess for Lorenz profile can be taken from the spectroscopy of D₂ line without Doppler broadening by running the simulation with atomic velocity equals to zero as shown in Fig. (3.5).

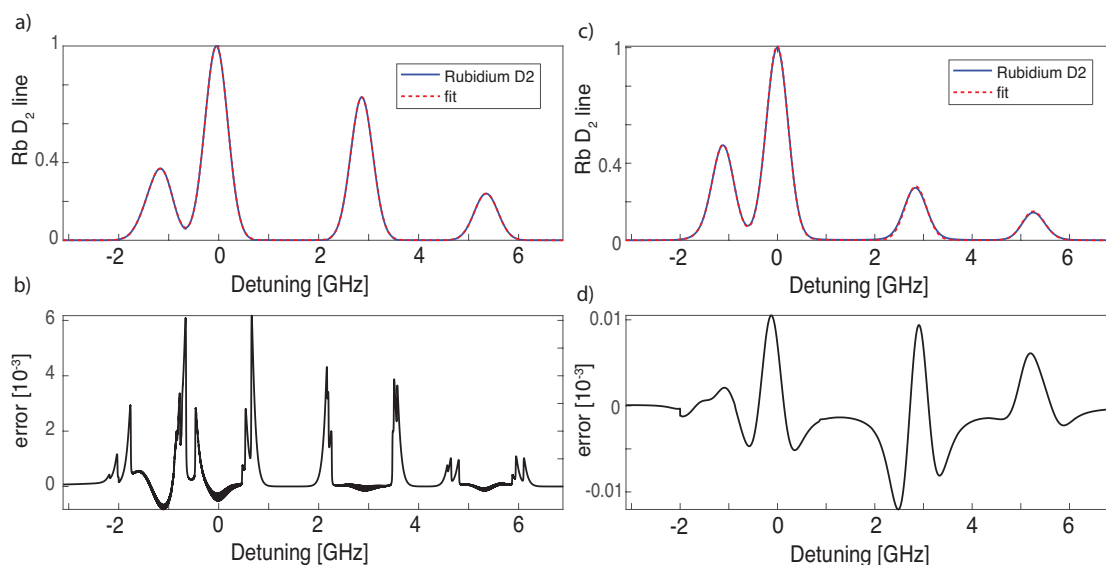


FIGURE 3.7: The figures a) b) at low intensity $I = 10^{-10} \text{ mW/cm}^2 \approx 2.8 \times 10^{-11} I_{\text{sat},87}$. The figures c) d) shows the fitting for D₂ line at $I = 10 I_{\text{sat},87}$. a) c) show the normalised induced dipole moment and b) d) show the residual error, a subtraction of the produced signal and the fit line.

The following figure shows a fitting example at high intensity $I = 10 I_{\text{sat},87}$. Compared to the low intensity one, the magnitude of residual error in high intensity

case is nearly one order of magnitude larger. Even then the fitting quality is acceptable with the residual error less than 1%. The fitting process with Faddeeva function provides 12 Lorentz FWHM for 12 possible transition of D_2 line. At low intensity, this Lorentz FWHM should approach the natural linewidth according to the equation (3.14). The natural Line Width is $(2\pi \cdot 6.0666 \text{ MHz})$ for ^{85}Rb [5] and $(2\pi \cdot 6.0659 \text{ MHz})$ for ^{87}Rb [6]. Since the width of two isotopes are close to each other, it is appropriate to expect those 12 values of Lorentz FWHM only have little differences resulting from fitting and then take the average value for the saturation intensity calculation later.

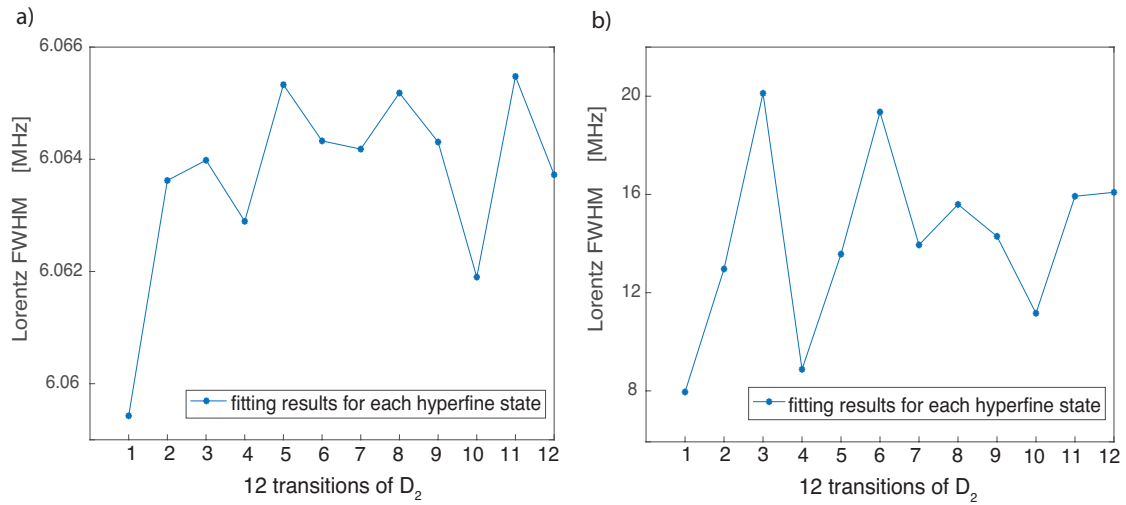


FIGURE 3.8: a) shows the lorentz FWHM at low intensity $I = 10^{-10} \text{ mW/cm}^2 \approx 2.8 \times 10^{-11} I_{\text{sat},87}$. and b) corresponds to higher intensity $I = 10 I_{\text{sat},87}$. These indices correspond to the indices in Fig. 3.5.

The standard deviation of all Voigt-fitting results is below 4%. The values for the cyclic transition in ^{87}Rb are given in the table below.

Intensity	10^{-10} W/m^2	$0.01 \times I_{\text{sat}}$	$0.1 \times I_{\text{sat}}$	I_{sat}	$10 \times I_{\text{sat}}$
FWHM of Lorentz [MHz]	6.063	6.094	6.344	8.452	20.079

TABLE 3.3: Lorentz FWHM for the cyclic transition in ^{87}Rb at different intensities

The fitting to discrete points gives the saturation intensity $I_{\text{sat}} = 3.564 \text{ mW/cm}^2$. This value is close to the expected value $I_{\text{sat},87} = 3.576 \text{ mW/cm}^2$.

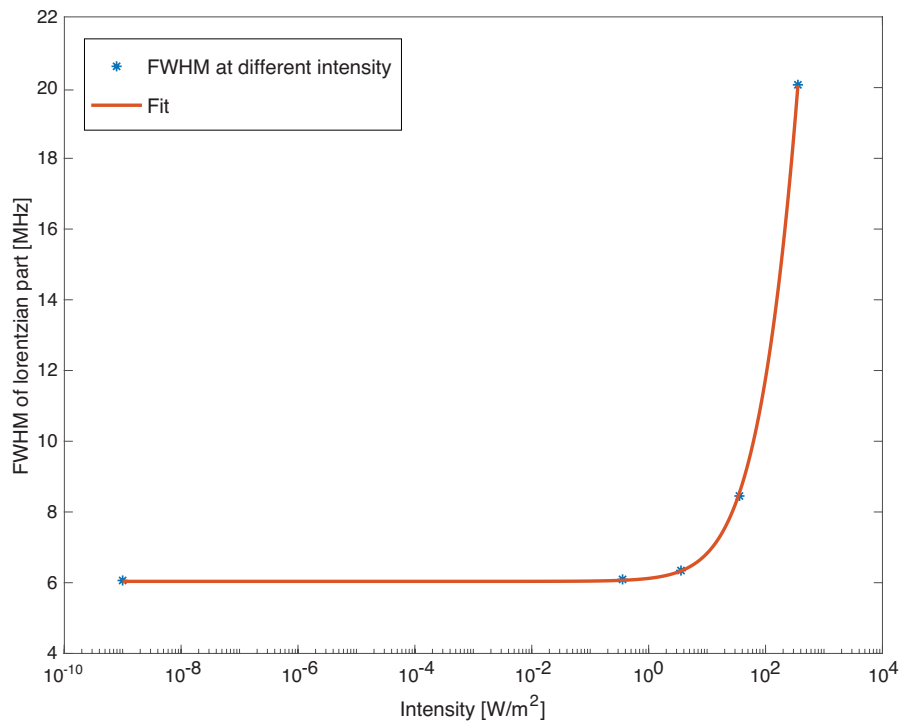


FIGURE 3.9: The five blue discrete stars are FWHM of transition $^{87}\text{Rb } |5S_{1/2}, F = 2\rangle \rightarrow |5P_{3/2}, F' = 3\rangle$ at different intensities from individual Voigt-fitting result. It shows the intensity-dependence of Lorentz FWHM. The x-axis is in logarithmic scale and a Fit (red line) gives the saturation intensity behavior.

4 Two-photon spectroscopy

In this chapter we use the counter-propagating 780 nm and 1529 nm (telecom) lasers to excite rubidium atoms from $|5S_{1/2}\rangle$ to $|5P_{1/2}\rangle$ then to $|4D_{5/2}\rangle$. First we present the experimental results followed by detailed analysis to extract the effect of the telecom power. Later, we employ our Matlab code and extend it to include $5P_{3/2} \rightarrow 4D_{5/2}$ transitions. We compare the results of those numerical simulations with our experimental results. At the end, we analyse the spectrum at different polarization.

4.1 Excitation scheme and experimental Setup

Figure (4.1) shows the schematics of the setup we used for two-photon spectroscopy of Rubidium. A 780 nm laser light passes through a dichroic mirror and excites the atoms to the $5P_{3/2}$ state. A beam propagating in the opposite direction of 780 nm laser within the cell is the the telecom laser with wavelength at 1529 nm. It sends the excited atoms to $4D_{5/2}$ state. The transmitted light from this laser gets reflected from the dichroic mirror and sent to a Germanium detector to record the absorption of telecom laser. The 780 nm laser is locked to the transition $|5S_{1/2}, F = 3\rangle \rightarrow |5P_{3/2}, F = 4\rangle$ of ^{85}Rb and the 1529 nm laser is scanned over $4D_{5/2}$ energy levels.

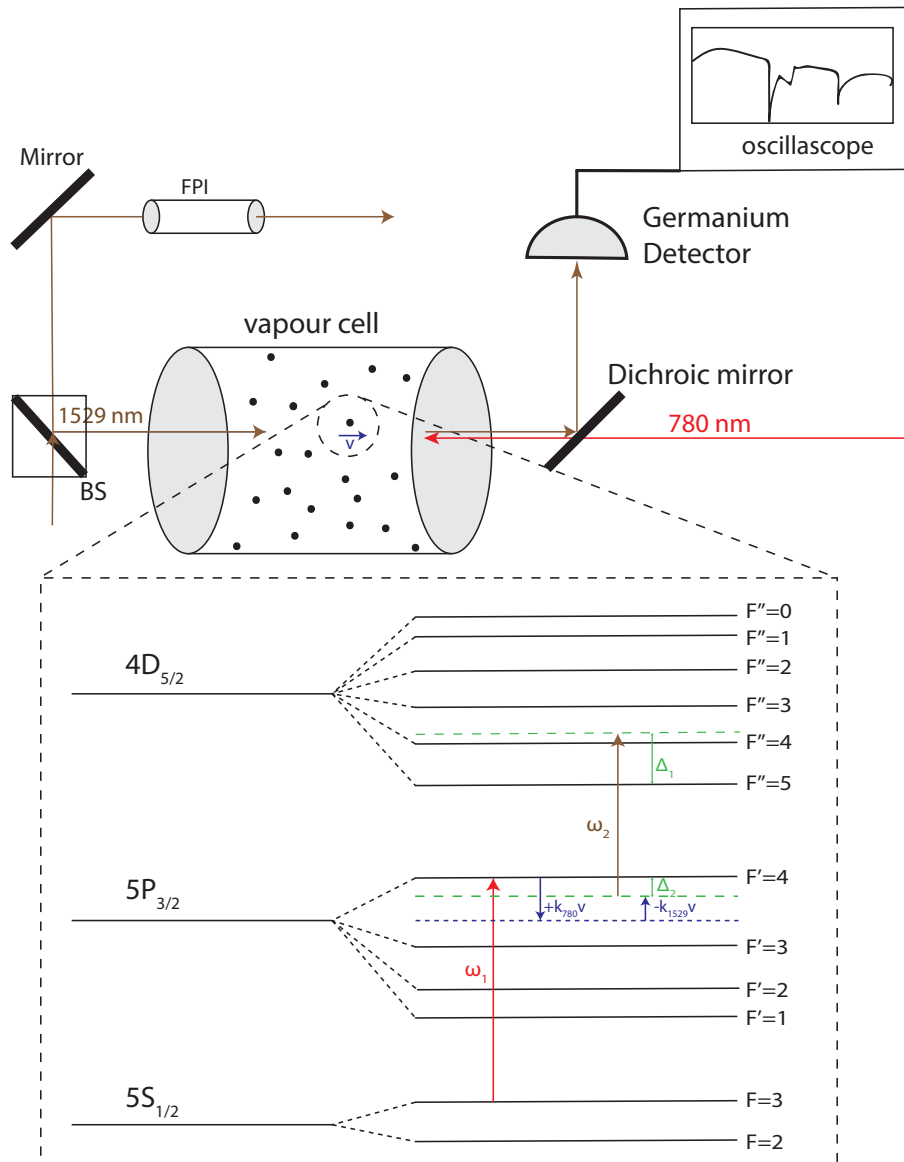


FIGURE 4.1: The experimental setup used for $|5S_{5/2}\rangle \rightarrow |5P_{5/2}\rangle \rightarrow |4D_{5/2}\rangle$ spectroscopy of Rubidium. The red arrow indicates the 780 nm laser with frequency ω_1 and the brown arrow indicates 1529 nm laser (telecom laser) used for transition $|5P_{3/2}\rangle \rightarrow |4D_{5/2}\rangle$ with frequency ω_2 . The Doppler detuning $(+k_{780}v - k_{1529}v)$ is dependent on the velocity of individual atoms. The real energy level that an atom reaches is shown in the dashed green line. The real detuning is the sum of Δ_1 and Δ_2 .

Several HWP (half-wave plate) + PBS (polarizing beam splitter) and ND filters (natural density filter) have been used to tune the intensity of 780 nm and the telecom laser.

The Doppler effect lets atom reach every hyperfine state of $5P_{3/2}$, even though the 780 nm laser is locked at $|5S_{1/2}, F = 3\rangle \rightarrow |5P_{3/2}, F' = 4\rangle$ transition. The 1529 nm telecom laser has a scanning range over several GHz to cover all hyperfine energy levels of $4D_{5/2}$ in ^{85}Rb . The spacing between peaks are presented in the table (4.1). The first line in table shows which transition a peak belongs to. $\Delta = 0$ corresponds to the cyclic transition of ^{85}Rb $|5S_{1/2}, F = 3\rangle \rightarrow |5P_{3/2}, F' = 4\rangle$. The spacing between transition peak 3-4-5, 3-4-4, 3-4-3 is the natural energy spacing. The spacing between $F \rightarrow F' \rightarrow F''$ and $F \rightarrow (F' - 1) \rightarrow F''$ is given by $(E_{F'} - E_{F'-1}) \times (1 - \frac{\lambda_1}{\lambda_2})$, where $\lambda_{1,2} = 2\pi \cdot c/\omega_{1,2}$ and E indicates the energy. For instance, the transition 3-3-4, 3-3-3, 3-3-2 are included in spectrum due to the doppler effect, and spacing between 3-3-4 and 3-4-4 is $120.64 \text{ MHz} \times (1 - \frac{780.24 \text{ nm}}{1529.37 \text{ nm}}) = 59.10 \text{ MHz}$ [11, 12].

Rubidium 85		Rubidium 87	
$F \rightarrow F' \rightarrow F''$	Δ [MHz]	$F \rightarrow F' \rightarrow F''$	Δ [MHz]
3-4-5	0	2-3-4	0
3-4-4	20.8	2-3-3	63.7
3-4-3	41.3	2-3-2	115.8
3-3-4	79.9	2-2-3	194.55
3-3-3	100.36	2-2-2	246.65
3-3-2	117.96	2-2-1	283.45
3-2-3	131.42	2-1-2	323.66
3-2-2	149.02	2-1-1	360.46
3-2-1	162.02		

TABLE 4.1: Spacing between different transition peaks.

The signal for data analysing is prepared by the subtraction of recorded absorption from a Ge-detector and the ramp-reference.

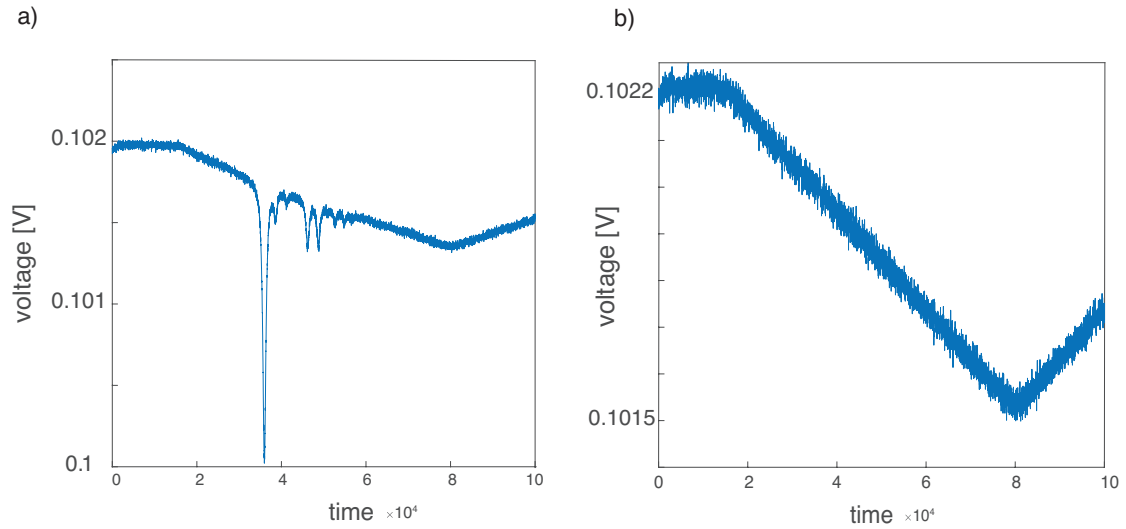


FIGURE 4.2: a) Original experimental data, the spectroscopy detecting by Ge-detector and b) background ramp.

The panel a) of Fig. (4.2) shows one absorption spectrum detected at a certain power $P_{780} \approx 20 \mu\text{W}$, $P_{1529} = 8.3 \mu\text{W}$. The panel b) shows the ramp signal, which is taken at the same telecom laser intensity but with the 780 nm laser being blocked. Because of the time difference between two measurements, the spectrum still has an unwanted offset. Hence, a polynomial is needed to exclude this background influence.

Via Fabry-Perot Interferometer the x-axis is calibrated to frequency. We checked the spacing between peaks 3-4-5 and 3-3-4 which should be 79.9 MHz [11].

After abstraction of the quadratic polynomial on signal and the normalization we obtain normalized transmission data, as Fig. (4.3) shows. In experiment we did in total 18 measurements with increasing 1529 nm laser power from $8.3 \mu\text{W}$ to $520 \mu\text{W}$. Fig. (4.3) exhibits five of them to show the power broadening clearly.

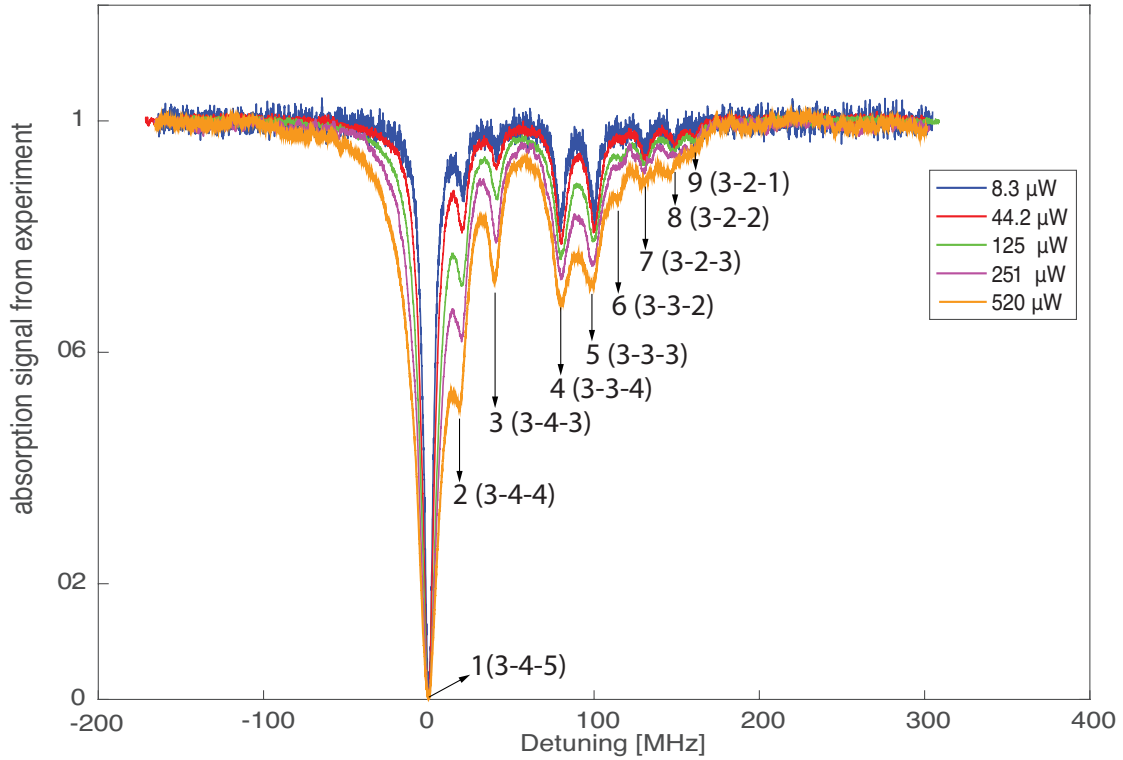


FIGURE 4.3: Normalised experimental signal with different powers. Numbers in legends indicate the power of 1529 nm laser.

The power of two beams are determined by power meter (Digital Optical Power and Energy Meter, PM100D). The power sensor S121C (type: Si Photodiode) is used for 780 nm laser, while power sensor S122C (type: Ge Photodiode) is used for 1529 nm laser. To calculate the exact intensity, two measurements are needed

- Generally, the power inside the vapour cell is less than the measured value because of the reflection loss. A measurement with blocked 780 nm laser shows that the 1529 nm laser power after the cell is 25% less than the power of the coming beam. Assuming the equal reflection on two sides of the cylindrical cell, the reflectance is 50%.
- The beam size measurement. From this measurement we know that the beam has Gaussian distribution with the diameter 1.42 mm. The intensity is calculated by dividing the power by the cross sectional area.

All the measurements are done at low 780 nm power to decrease the optical pumping and power broadening due to this beam.

4.1.1 Rabi frequency and saturation intensity of each transition

In chapter 2, we described how to calculate Rabi frequencies and induced dipole moments of transitions between hyperfine states. The saturation intensity for individual transition $F \rightarrow F' \rightarrow F''$ is calculated using the eq. (2.25). Table (4.2) presents the exact value that we used for those variables in simulation and gives the saturation intensity I_{sat} which can be compared with experimental results.

Rubidium 85			
index ($F \rightarrow F' \rightarrow F''$)	$C_q(q = 0, \pm 1)$	$d_{FF'} [ea_0]$	$I_{\text{sat}} [\text{mW}/\text{cm}^2]$
1 (3-4-5)	0.2716	2.9239	0.16950
2 (3-4-4)	0.0556	1.3224	0.82869
3(3-4-3)	0.0062	0.4408	7.45818
4(3-3-4)	0.2143	2.5971	0.21485
5 (3-3-3)	0.100	1.7742	0.46038
6 (3-3-2)	0.0190	0.7743	2.41700
7 (3-2-3)	0.1600	2.2442	0.28774
8 (3-2-2)	0.1333	2.0486	0.34529
9 (3-2-1)	0.0400	1.1221	1.15095
10* (2-1-2)	0.1037	1.8067	0.44394
11* (2-1-1)	0.1556	2.2128	0.29596
12* (2-1-0)	0.0741	1.5270	0.62152

TABLE 4.2: Rabi frequency prefactor C_q , and saturation intensity. Index with star means this transition is not seen in the experiment. As the 780 nm laser is locked for transition $|5S_{1/2}, F = 3\rangle \rightarrow |5P_{3/2}, F' = 4\rangle$, the population of state $|5P_{3/2}, F' = 1\rangle$ comes from the decaying of the $4D_{5/2}$ states, resulting in weak strength compared with others.

Table (4.3) shows the calculated dipole moment and saturation intensity for ^{87}Rb $4D_{5/2}$ excitation.

4.1.2 Calculation of branching ratio decay rates of hyperfine levels

Similar to the calculations for D_2 line, the decay rates of $4D_{5/2}$ hyperfine states are given by the product of branching ratio $B_{FF'}$ and the spontaneous decay rate $\Gamma(J = 3/2, J' = 5/2) = 2\pi \cdot 1.89 \text{ MHz}$ [5,6]. The calculated values can be found in the table (4.4).

Rubidium 87			
$F' \rightarrow F''$	$C_q(q = 0, \pm 1)$	$d_{FF'} [ea_0]$	$I_{\text{sat}} [\text{mW}/\text{cm}^2]$
3-4	0.2857	2.9989	0.16113
3-3	0.0444	1.1828	1.03586
3-2	0.0032	0.3161	14.5020
2-3	0.2489	2.7990	0.18497
2-2	0.0778	1.5647	0.59192
2-1	0.0067	0.4581	6.90573
1-2	0.2333	2.7101	0.19731
1-1	0.1000	1.7742	0.46038
0-1	0.3333	3.2392	0.13811

TABLE 4.3: Rabi frequency prefactor C_q , and saturation intensity. Actually the peaks caused by excitation in ^{87}Rb is not seen in the spectrum due to the off-resonance effect.

^{85}Rb		^{87}Rb	
$ 5P_{3/2}, F'\rangle \rightarrow 4D_{5/2}, F''\rangle$	$B_{FF'}$	$ 5P_{3/2}, F'\rangle \rightarrow 4D_{5/2}, F''\rangle$	$B_{FF'}$
$F' = 4 \rightarrow F'' = 5$	1	$F' = 3 \rightarrow F'' = 4$	1
$F' = 3 \rightarrow F'' = 4$	0.75	$F' = 2 \rightarrow F'' = 3$	0.8
$F' = 4 \rightarrow F'' = 4$	0.25	$F' = 3 \rightarrow F'' = 3$	0.2
$F' = 2 \rightarrow F'' = 3$	0.5143	$F' = 1 \rightarrow F'' = 2$	0.63
$F' = 3 \rightarrow F'' = 3$	0.45	$F' = 2 \rightarrow F'' = 2$	0.35
$F' = 4 \rightarrow F'' = 3$	0.0357	$F' = 3 \rightarrow F'' = 2$	0.02
$F' = 1 \rightarrow F'' = 2$	0.28	$F' = 0 \rightarrow F'' = 1$	0.5
$F' = 2 \rightarrow F'' = 2$	0.6	$F' = 1 \rightarrow F'' = 1$	0.45
$F' = 3 \rightarrow F'' = 2$	0.12	$F' = 2 \rightarrow F'' = 1$	0.05
$F' = 1 \rightarrow F'' = 1$	0.7		
$F' = 2 \rightarrow F'' = 1$	0.3		
$F' = 1 \rightarrow F'' = 0$	1		

TABLE 4.4: Branching ratio for transitions $5P_{3/2}$ to $5D_{5/2}$ in hyperfine structure

4.1.3 Fitting results

The multi-Lorentz fit, i.e. a sum of 9 Lorentz function, is used for the fitting the two-photon spectrum. In total there are 9 peaks with 9 Lorentz FWHM. The fitting for the cyclic transition (3-4-5) has the best quality since it has strongest strength.

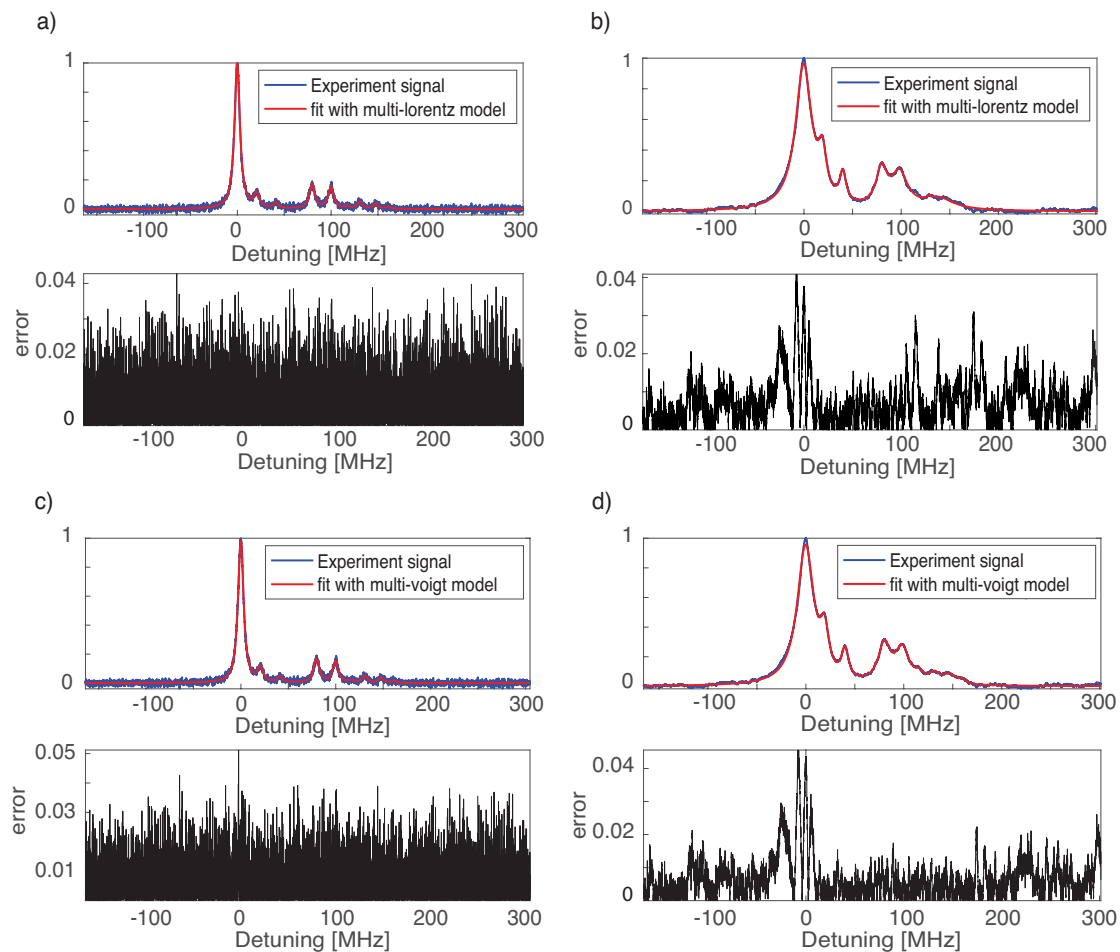


FIGURE 4.4: Penal a) shows the Lorentz fit result at relative low telecom Power $P = 8.3 \mu\text{W}$. Penal b) shows the Lorentz fit result at high 1529 nm laser power $P = 520 \mu\text{W}$. Penal c) shows the Voigt fit result at $P = 8.3 \mu\text{W} \approx 0.77P_{\text{sat}}$ and penal d) shows the Voigt Fit result at $P = 520 \mu\text{W} \approx 48.5P_{\text{sat}}$. In each penal, the upper part shows the fit curve (red) on top of experimental data (blue) and the lower part shows the absolute error calculated as $|S_{\text{fit}} - S_{\text{exp. data}}|$ (S means signal).

Both fits seem to describe the data properly with a relatively low error. However, the Lorentz fit for the third group transition (3-2-3, 3-2-2, 3-2-1) and the third transition 3-3-2 in second group was not giving the exact value of Lorentz width since the fit starts to have difficulties to detect the peak, which has broad width and small height. In addition, a Voigt fit is closer to the real behavior of the data since the Doppler effect is not negligible. The Doppler width Γ_d is given by the product of the natural line-width of $5P_{3/2}$ state $\Gamma_{5P} = 6.066 \text{ MHz}$ [5] and ratio

between wave number of 780 nm and 1529 nm laser [13].

$$\Gamma_d = \frac{k_{1529}}{k_{780}} \cdot \Gamma_{5P} \approx 3.049 \text{ MHz} \quad (4.1)$$

Fig. (4.5) shows the Lorentz FWHM from Lorentz Fit for transition 3-4-5, 3-4-4, 3-4-3, 3-3-4, 3-3-3. At low intensity, the Lorentz FWHM for each transition are close to each other. Theoretically, FWHM for all transitions would approach the sum of the natural linewidth and an offset coming from background according to the equation (2.30). At higher Power, the FWHMs increase differently because of different I_{sat} values of each transition.

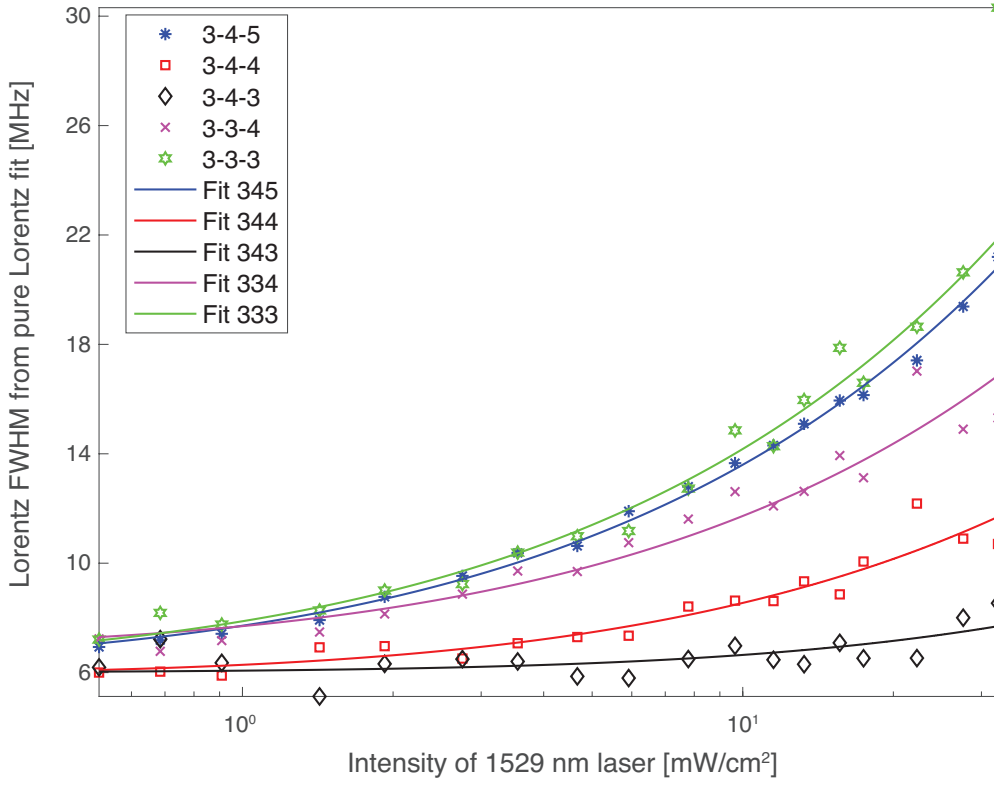


FIGURE 4.5: FWHM of Lorentz using the pure Lorentz fit for isotope ^{85}Rb . The excitation in ^{87}Rb is off-resonance. Hence this fit model is a multi-Lorentz model with a superposition of 9 Lorentz function

The saturation intensity I_{sat} obtained by the Lorentz Fit and the offset Γ_0 are presented in table (4.5).

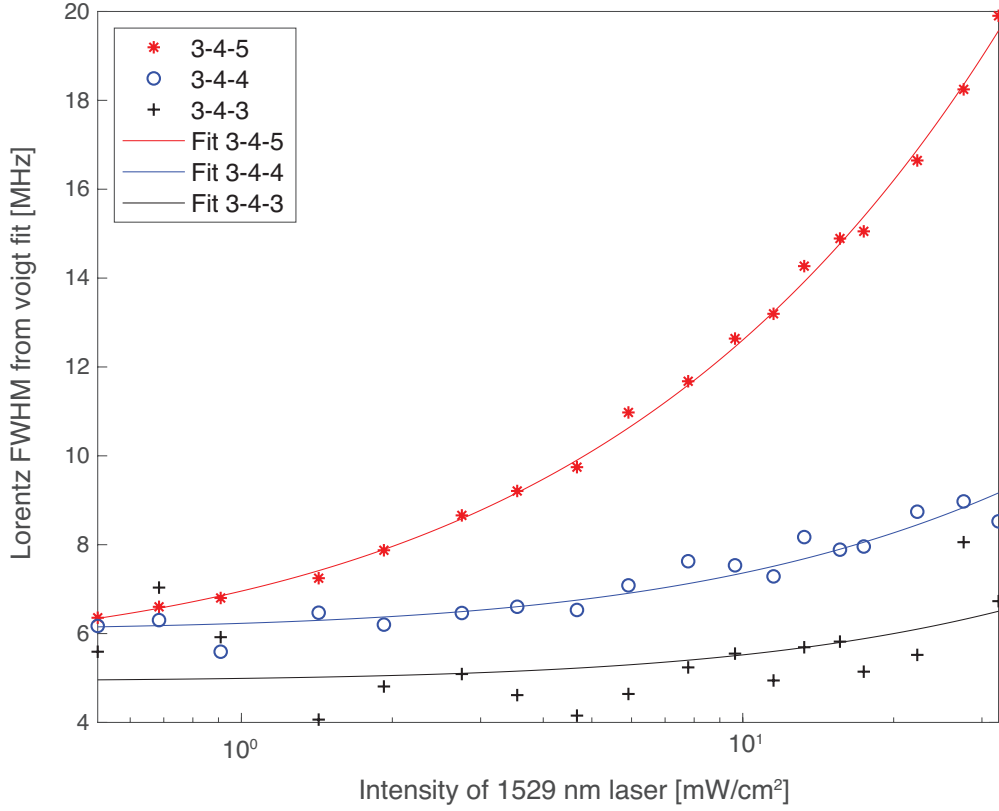


FIGURE 4.6: FWHM of Lorentz using the Voigt Fit (faddeeva function)

From the FWHM of Lorentz part in Voigt fitting, the saturation intensity could be determined by Fitting with function (2.30) .

$F - F' - F''$	$I_{\text{sat,theo}}$	$I_{\text{sat, voigt}}$	$\Gamma_{0,\text{voigt}}$	$I_{\text{sat, lor}}$	$\Gamma_{0,\text{lor}}$
3-4-5	0.1695	0.3363	3.032	0.3884	4.323
3-4-4	0.82869	2.97	3.862	2.592	4.379
3-4-3	7.45818	5.017	2.187	7.957	3.987
3-3-4	0.21485	0.5683	3.152	0.8568	4.828
3-3-3	0.46038	0.5271	3.428	0.86	5.349
3-3-2	2.417	3.597	4	-	-
3-2-3	0.28774	0.8299	2.359	-	-
3-2-2	0.34529	0.3751	1.646	-	-
3-2-1	1.15095	2.173	2	-	-

TABLE 4.5: Evaluated value for I_{sat} calculation. The unit of I_{sat} is mW/cm^2 . The minus symbol means this result is not reasonable due to the bad fit quality when the intensity is low.

4.2 Comparison between the experiment and the simulation

We compare the experimental and simulation results at low intensity. As the strength of each transition is sensitive to the intensity of both laser beams, we simulate the spectrum with increasing 780 nm laser intensity and at fixed 1529 nm laser intensity vice versa. Fig. (4.7) shows the power broadening effecting on the peaks strength and widths.

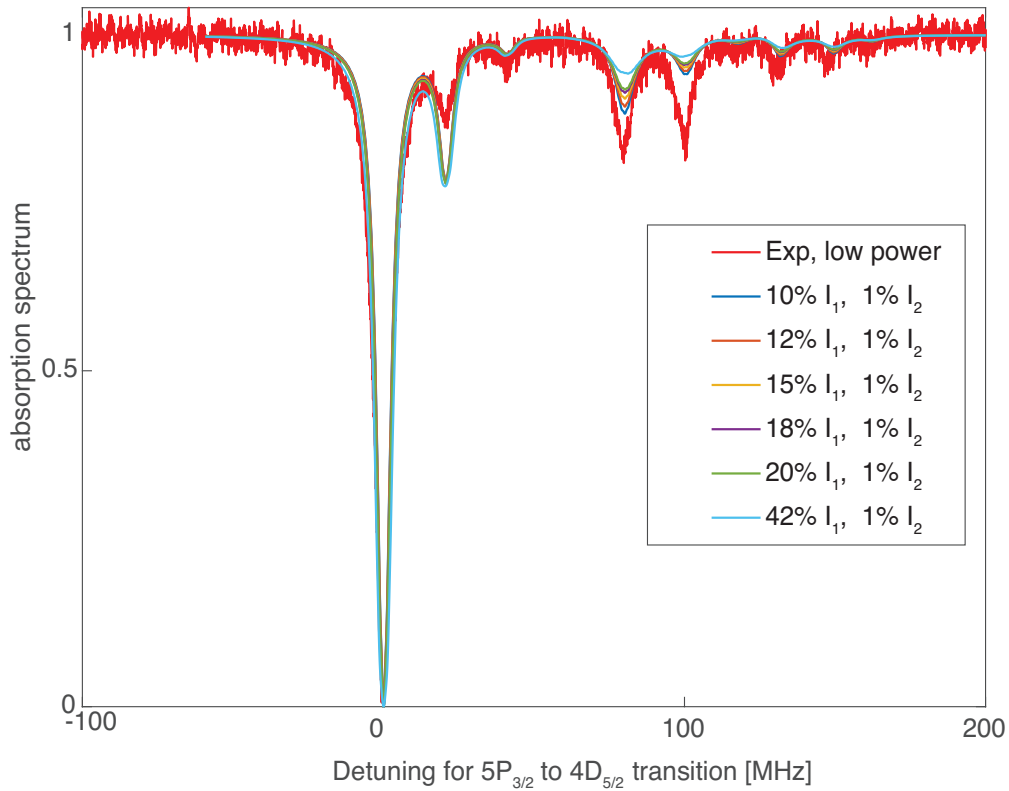


FIGURE 4.7: Spectra with increasing intensity of 780 nm laser. The legend includes $I_1 = 3.576$ mW/cm², $I_2 = 1.695$ mW/cm². The experimental result corresponds to the measurement at low power: $P_{780} \approx 20$ μ W, $P_{1529} \approx 8.3$ μ W.

We find out that the experimental data can be in good agreement with simulation when $I_{780} = 5\%$ I_1 and $I_{1529} = 5\%$ I_2 . Fig. (4.8) shows this comparison.

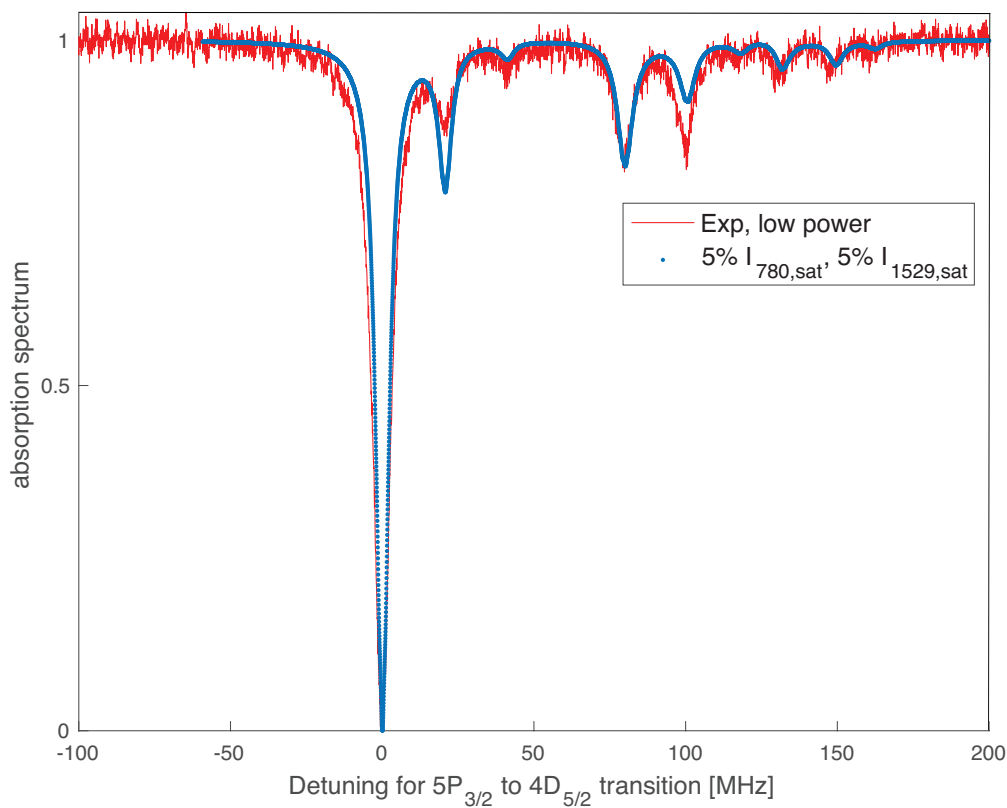


FIGURE 4.8: Comparison for low power case. The absorption spectrum produced by simulation at $I_{780} = 5\% I_1$ and $I_{1529} = 5\% I_2$ is compared with the experimental data at $P_{780} \approx 20 \mu\text{W}$, $P_{1529} = 8.3 \mu\text{W}$.

However, some of the peaks are still not in perfect agreement with the experimental data. A fact that can be attributed to the polarization effect as will be discussed in the next section.

4.3 Polarization effect

It should be mentioned that the polarization of laser beam affects the spectrum. Especially for transition 3-4-4 and 3-3-3, the strength of absorption (induced dipole moment) turns to be different for π or σ^\pm transitions. Fig. (4.9) shows how the polarisation of 780 nm beam changes the spectroscopy.

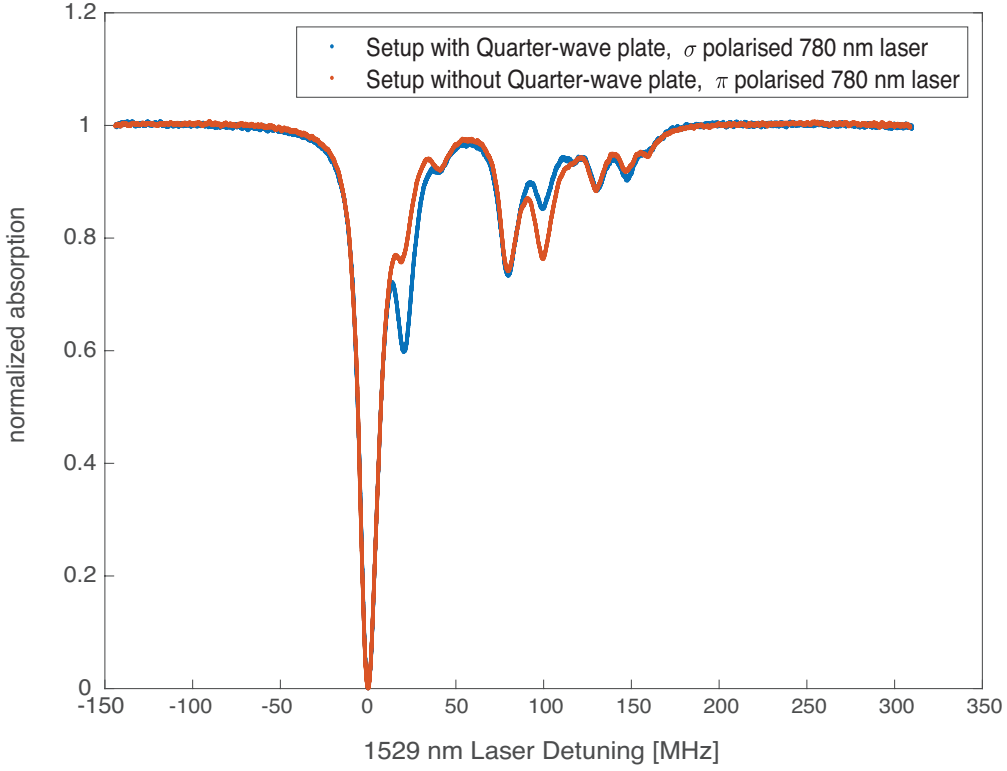


FIGURE 4.9: Polarisation changes the peaks height. Using a QWP in 780 nm path the polarization of pump beam has been changed from linear to circular (blue). As one can see the spectrum is noticeably different from the linear case (red line).

From this figure, we notice that the second peak in each group changes its height obviously. This phenomenon is similar to what we have in the comparison between the experiment and simulation. To capture this polarization effect one has to develop a more detailed model including all Zeeman sub-levels with polarization-sensitive Rabi frequencies. That leads to a density matrix of 72×72 (total number of Zeeman sub-levels in $5S_{1/2} \rightarrow 5P_{3/2} \rightarrow 4D_{5/2}$ structure) for ^{85}Rb and 48×48 for ^{87}Rb . The Rabi frequency is given by

$$\Omega_{m_F, m_{F'}} = \frac{\sqrt{C_{m_F, m_{F'}}^2 / (2F + 1) \cdot |\langle J || \hat{\mathbf{d}} || J' \rangle| \cdot E}}{\hbar} \quad (4.2)$$

The decay rate $\Gamma_{m_F, m_{F'}}$ and branching ratio $B_{m_F, m_{F'}}$ for each transition between two Zeeman sub-level $|F, m_F\rangle$ and $|F', m_{F'}\rangle$ can be written as

$$B_{m_F, m_{F'}} = \frac{2J' + 1}{2J + 1} \cdot C_{m_F, m_{F'}}^2 \cdot \frac{1}{2F' + 1} \quad (4.3)$$

$$\Gamma_{m_F, m_{F'}} = B_{m_F, m_{F'}} \cdot \Gamma(J, J') \quad (4.4)$$

where $C_{m_F, m_{F'}}^2$ is the specific Zeeman sub-level strength for the transition $|F, m_F\rangle \rightarrow |F', m_{F'}\rangle$. The primed letters indicate excited state levels. Applying these Rabi frequencies and decay rates into the optical Bloch equations, one can calculate the accurate density matrix involving 72 or 48 Zeeman sub-levels.

5 Summary and Outlook

In this thesis, we modeled a 12-level system (10-level system) for ^{85}Rb (^{87}Rb) hyperfine structure and analyse the two-photon spectroscopy with counter-propagating lasers. By running the code we obtain the two-photon spectrum at certain intensity and beam size. In chapter 3 we produced the D_2 line with MATLAB simulation and compared it with the Elecsus data. A new fitting method using Faddeeva function and `lsqnonlin` (a MATLAB built-in solver) is also introduced and tested by the behavior of power broadening effect. An experimental setup is constituted to investigate the two-photon spectroscopy. We compared the fit results using Lorentz fit and Voigt fit by analysing the line broadening effect. Afterwards, the experimental and simulation spectra at low intensity are compared with each other. From this comparison, we found small difference in strengths of several transitions. With the experiment with π and σ polarised laser light we believe that one reason for this difference is the polarization of the light. The way to construct an improved simulation model is given at the end of chapter 4. It takes the transition strength of all Zeeman sub-levels to account and calculates the polarization-sensitive susceptibility.

In this chapter, we will give two examples for further works using the MATLAB simulation.

5.1 Time-dependent behaviour

As the pseudo steady-state simulation can not describe the waveguide geometry and some other properties, we need to use the Monte-Carlo simulation to model the atom-light interaction. In that simulation we assume that atoms are distributed randomly in the vapour cell and consider the velocity distribution. The time-dependence of population for each state is important for moving atoms in the vicinity of devices [14].

To obtain the time-dependent population we need to solve the optical Bloch equations for 12-level system in ^{85}Rb and 10-level system in ^{87}Rb , i.e. the extended form of eq. (2.12) to (2.15). The figures show the time-dependence of the population of each hyperfine level.

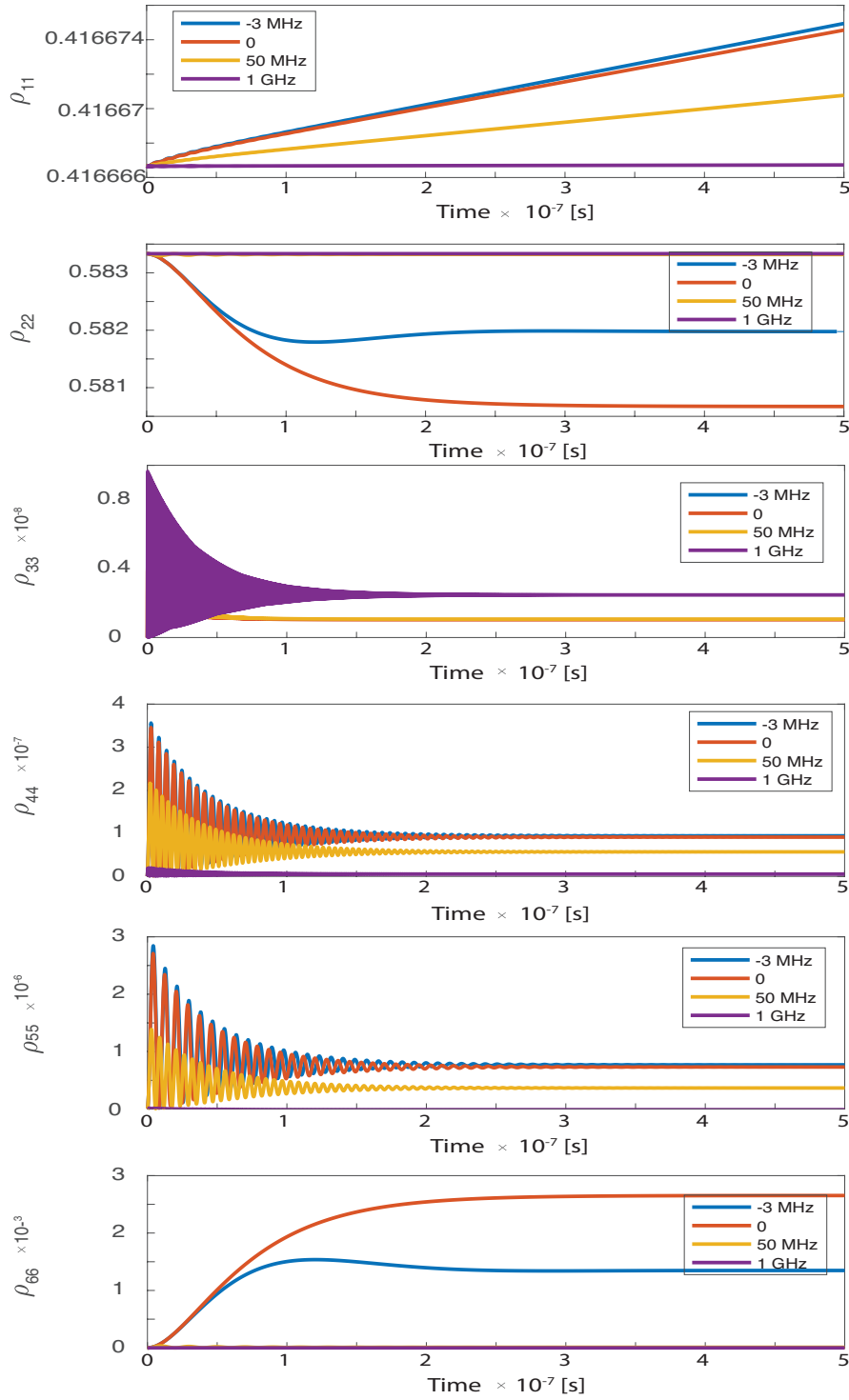


FIGURE 5.1: Time-dependent population change with different detuning, the legends show the Detuning of transition $|5S_{1/2}, F = 3\rangle \rightarrow |5P_{3/2}, F' = 4\rangle$. ρ depicts the population and the index depicts the level. For instance, ρ_{11} is the population for $|5S_{2/1}, F = 2\rangle$, and it is the (1,1)-element in the density matrix.

The signals in Fig. (5.1) are generated by the time-dependent code, using the time step $dt = 0.05$ ns and a time limit at 500 ns. The temperature is set to 20°C. We assume the atomic velocity to be zero to simplify this task and reduce the running time for the MATLAB calculating process.

The curves in figure correspond to the population of each involved hyperfine energy level. In our simulation, they are the diagonal matrix entries of the density matrix in the multi-level scheme. At the beginning, the atoms are distributed in the two ground states $|5S_{1/2}, F = 2\rangle$ and $|5S_{1/2}, F = 3\rangle$. The probabilities of occupancy of each Zeeman sub-levels in these two states are equal. Therefore, at the beginning the population of $|5S_{1/2}, F = 2\rangle$ is 5/12 and of $|5S_{1/2}, F = 3\rangle$ is 7/12. Once the pump process starts, the population of the dark state $|5S_{1/2}, F = 2\rangle$ increases due to the optical pumping, while the population of $|5S_{1/2}, F = 3\rangle$ decreases as some atom are excited to the $5P_{3/2}$ levels. When the detuning is zero, the population of the state $|5P_{3/2}, F' = 4\rangle$ increase to around 2.5×10^{-3} after 500 ns. It is higher than other population in $5P_{3/2}$ levels since for zero detuning, because $|5S_{1/2}, F = 3\rangle \rightarrow |5P_{3/2}, F' = 4\rangle$ is the cyclic transition.

When the transition $|5P_{3/2}\rangle \rightarrow |4D_{5/2}\rangle$ is considered in the time-dependent simulation, we obtain the population change of all 12 transitions for ^{85}Rb , as Fig. (5.2) to (5.4) show. We set intensity $I_{780} = 0.1788$ mW/cm² and $I_{1529} = 0.008475$ mW/cm². The temperature is 40°C.

Similar to the fig. (5.1), the population of the dark state (ρ_{11}) increases over time. In some figures, the curves are overlapped with each other, means no huge differences between different Detuning settings. For $4D_{5/2}$ levels, the population of $4D_{5/2}, F'' = 5, 4$ are larger than others (especially for $\Delta = 0$).

At zero detuning, the 780 nm laser pumps atom from $|5S_{1/2}, F = 3\rangle$ to $|5P_{3/2}, F' = 4\rangle$, and it results in the decrease in population ρ_{22} and correspondingly the increase of population ρ_{66} . The excitation of 1529 nm laser leads to the increase of population ρ_{77} , which depicts the population of the state $|4D_{5/2}, F'' = 5\rangle$.

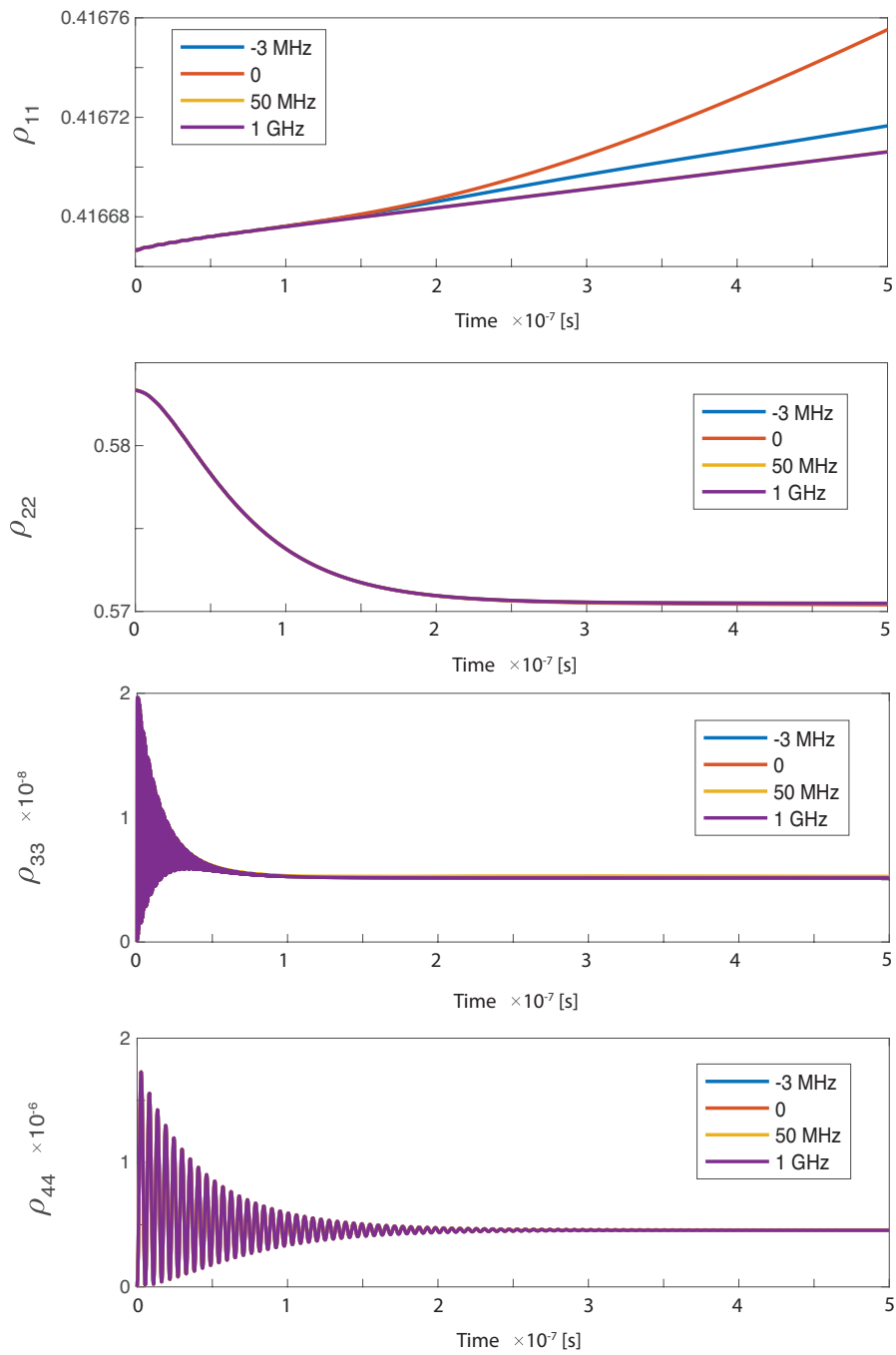


FIGURE 5.2: Time-dependent population change of first four energy levels, the legends show the Detuning of transition $|5P_{3/2}, F' = 4\rangle \rightarrow |4D_{3/2}, F'' = 5\rangle$

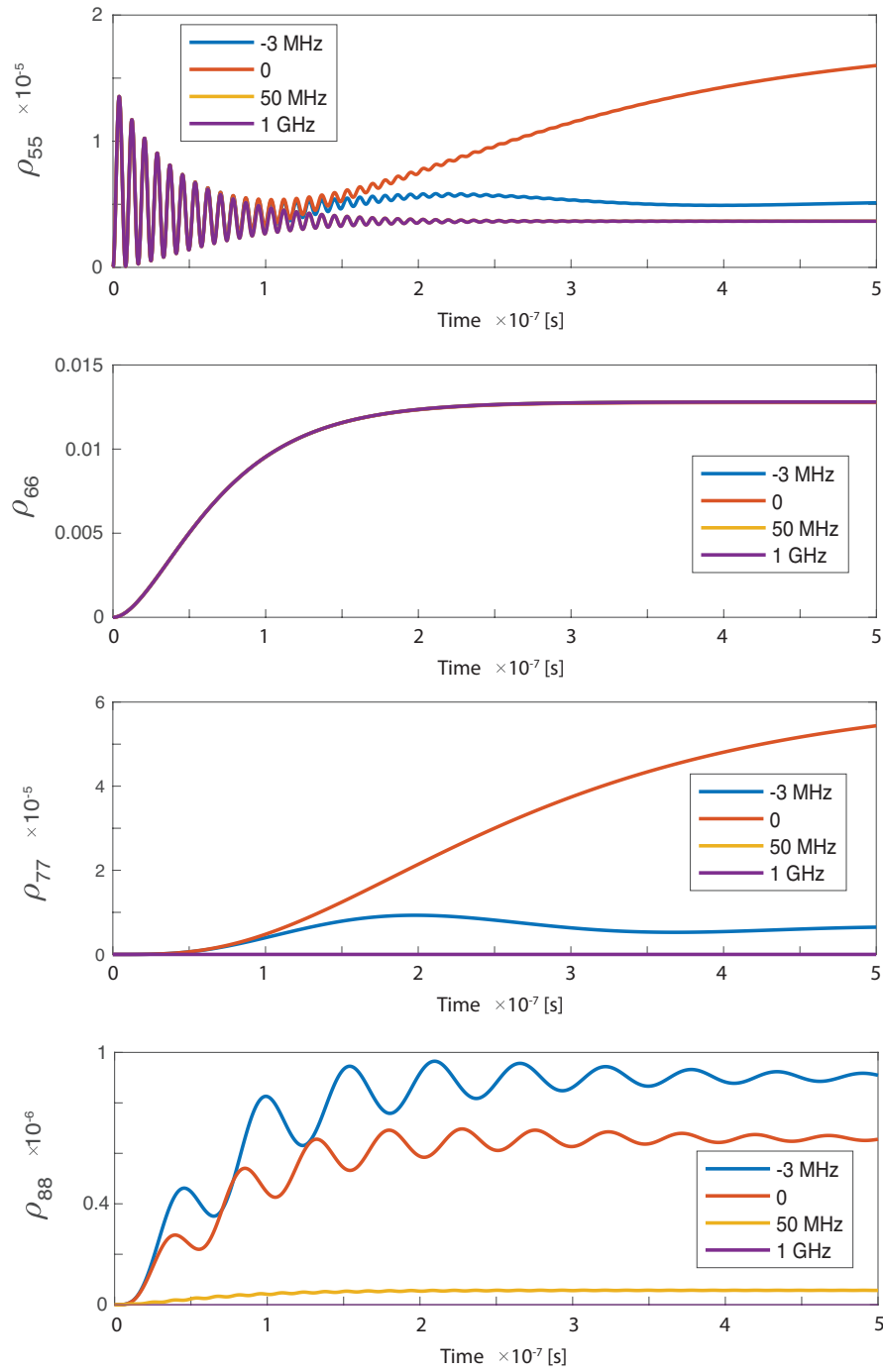


FIGURE 5.3: Time-dependent population change of the fifth to eighth energy levels, the legends show the Detuning of transition $|5P_{3/2}, F' = 4\rangle \rightarrow |4D_{3/2}, F'' = 5\rangle$

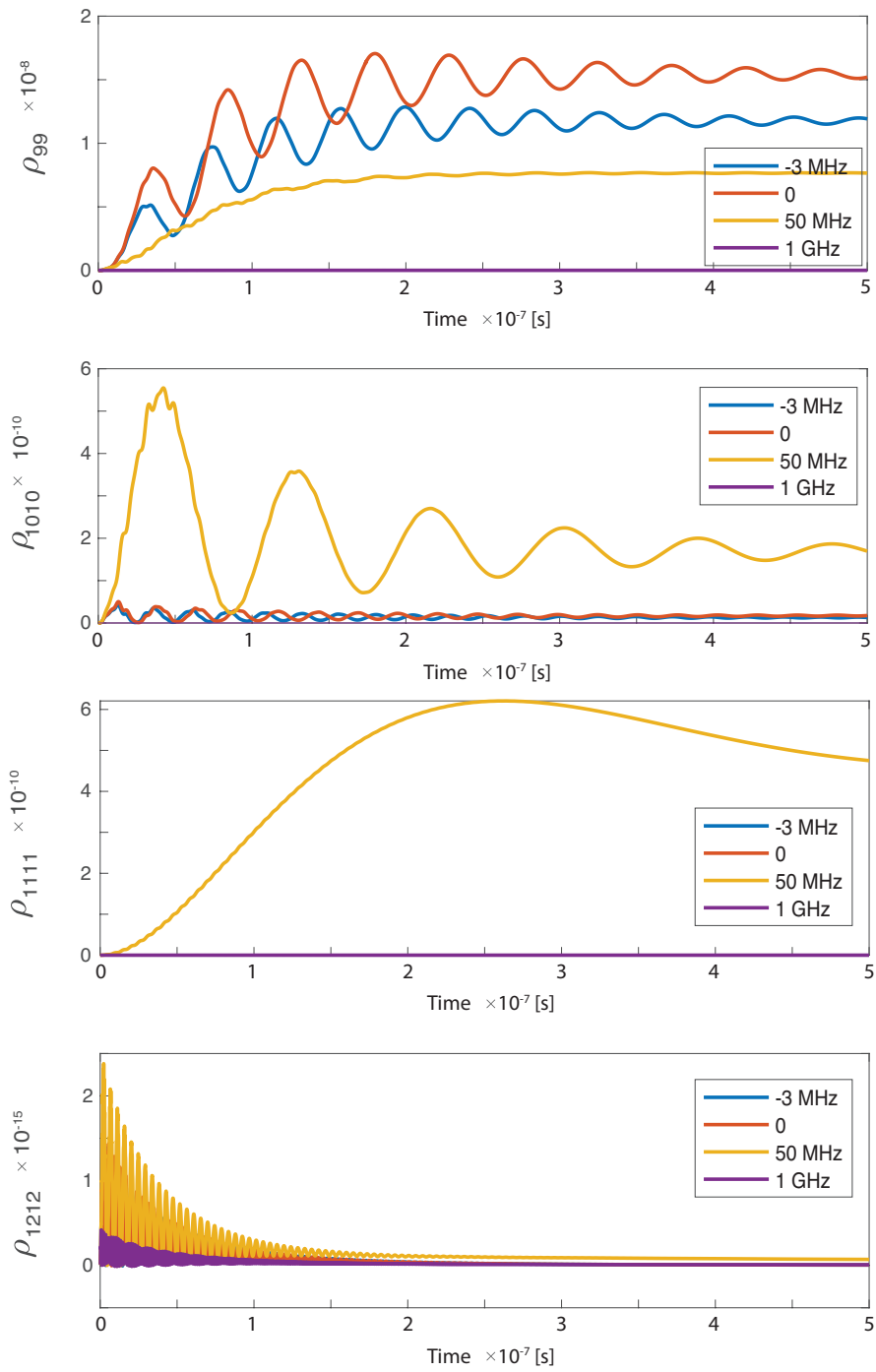


FIGURE 5.4: Time-dependent population change of last four energy levels, the legends show the Detuning of transition $|5P_{3/2}, F' = 4\rangle \rightarrow |4D_{3/2}, F'' = 5\rangle$

5.2 Two-dimensional color map

A two-dimensional color map for two-photon spectroscopy is produced by setting different detunings of transitions $|5S_{1/2}\rangle \rightarrow |5P_{3/2}\rangle$ and $|5P_{3/2}\rangle \rightarrow |4D_{5/2}\rangle$. The map can be used for the determination of correct detuning in experiment. We produce the map of the induced dipole moment. At low intensity the strength of dipole moment is small enough to approximate the transmission map. In our simulation, we scanned the 780 nm laser from -2 to 8 GHz and scanned the 1529 nm laser with a step of 15 MHz.

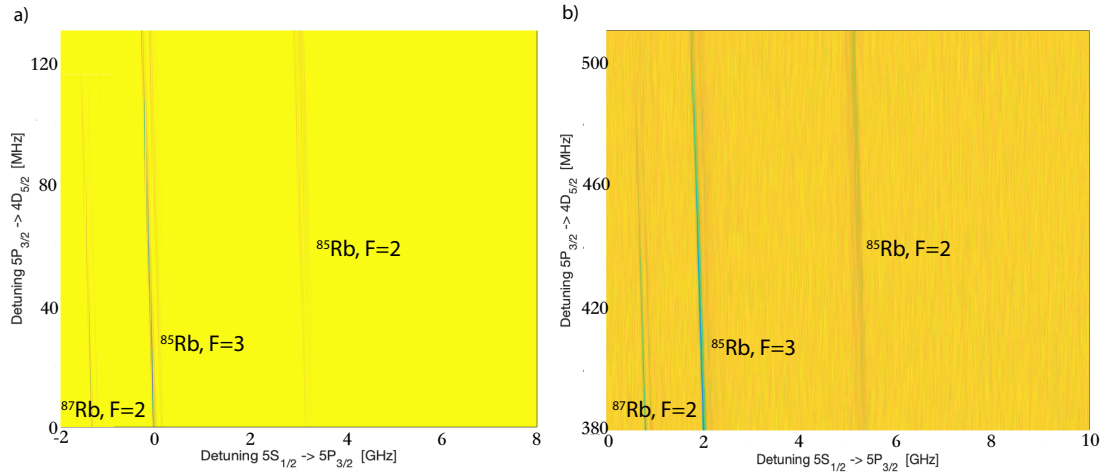


FIGURE 5.5: Two-dimensional color maps. Panel a) shows the result of our simulation. In x-axis, the detuning=0 corresponds to the transition $|5S_{1/2}, F=3\rangle \rightarrow |5P_{3/2}, F'=4\rangle$ of ^{85}Rb , while in y-axis the zero detuning corresponds to the transition $|5P_{3/2}, F=4\rangle \rightarrow |4D_{5/2}, F''=5\rangle$ of ^{85}Rb . The labels near the lines indicate that which ground state of which isotope the lines correspond to. Panel c) shows the experimental result with a scanning range of 10 GHz for 780 nm laser and 800 MHz for 1529 nm laser. The axis tick labels are different because in experiment the zero detuning was not chosen as the cyclic transition. Panel b) shows the experimental results. The experimental data were offered by a group in IHFG (Institut für Halbleitertechnik und Funktionelle Grenzflächen). In their research, the 1529 nm laser was scanned with 7 MHz steps. Two laser lights were π -polarised.

The following figure shows the complete map from the experiment. By choosing the detuning range appropriately, the zoom-in version, i.e. panel b) of Fig. (5.5) is obtained.

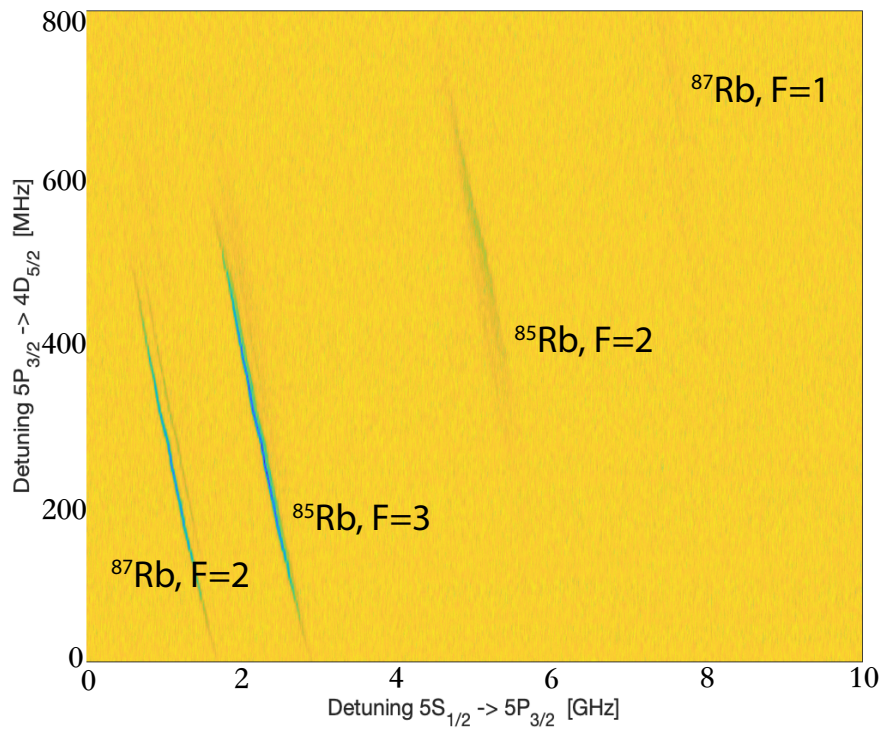


FIGURE 5.6: Complete two-dimensional color map from the experiment

Compared to our simulated color map, the slopes of simulation result and experiment result are the same. A more quantitative comparison between our simulation and experiment is the subject of further follow up studies.

Bibliography

- [1] D.A.Steck. Quantum and atom optics, 2006. available online at <http://steck.us/teaching>.
- [2] W.Demtröder. *Laser Spectroscopy Vol.1*. Springer, 2008.
- [3] J. J. Olivero and R. L. Longbothum. Empirical fits to the voigt line width: A brief review. *Journal of Quantitative Spectroscopy and Radiative Transfer*, 17:233–236, 2009.
- [4] J Sagle, R K Namiotka, and J Huennekens. Measurement and modelling of intensity dependent absorption and transit relaxation on the cesium d1 line. *J. Phys. B: At. Mol. Opt. Phys.*, 29:2629–2643, 1996.
- [5] D.A.Steck. Rubidium 85 d line data, 2013. available online at <http://steck.us/alkalidata>, Version 2.1.6.
- [6] D.A.Steck. Rubidium 87 d line data, 2015. available online at <http://steck.us/alkalidata>, Version 2.1.5.
- [7] Paul Siddons, Charles S Adams, Chang Ge, and Ifan G Hughes. Absolute absorption on rubidium d lines: comparison between theory and experiment. *J. Phys. B: At. Mol. Opt. Phys.*, 41(15), 2008.
- [8] A.V.Masalova and V.G.Minogin. Spontaneous decay rates of the hyperfine structure atomic states into an optical nanofiber. *JETP*, 118(5), 2014.
- [9] Mark A. Zentile, James Keaveney, Lee Weller, Daniel J. Whiting, Charles S. Adams, and Ifan G. Hughes. Elecsus: A program to calculate the electric susceptibility of an atomic ensemble. *Computer Physics Communications*, 189:162–174, 2015.
- [10] S.M. Abrarov and B.M. Quine. Efficient algorithmic implementation of the voigt complex error function based on exponential series approximation. *Applied Mathematics and Computation*, 218:1894–1902, 2011.

- [11] Jie Wang, Huifeng Liu, Guang Yang, Baodong Yang, and Junmin Wang. Determination of the hyperfine structure constants of the 87rb and 85rb 4d5/2 state and the isotope hyperfine anomaly. *Phys. Rev. A*, 90, 2014.
- [12] A. Urvoy, C. Adams K. Weatherill C. Carr, R. Ritter, and R. Löw. Opticalcoherences and wavelength mismatch in ladder systems. *J. Phys. B*, 46:36–94, 2013.
- [13] A. Skljarow. Evanescent two photon spectroscopy of rubidium atoms for integrated silicon structures at telecom wavelength, 2018.
- [14] R. Ritter. Interfacing thermal atoms with integrated photonic waveguides, 2018.

Acknowledgements

First of all, I would like to thank Prof. Dr. Tilman Pfau for offering me the opportunity to do my bachelor thesis at the 5th Physical Institute.

I would like to express my great appreciation to Dr. Hadiseh Alaeian who keeps encouraging me and spends lots of time teaching me how to do scientific research correctly. Thank you very much for your patience.

Thanks to Dr. Robert Löw, Dr. Harald Kübler, Dr. Mark Zentile for giving me many helpful suggestions.

I thank Artur Skljarow for teaching me how to do the laser experiment properly and helping me with MATLAB problems.

Thanks to Dr. Mark Zentile, Ioannis Caltzidis for helping me to understand Elecsus program.

Thanks to Hüseyin Vural, Julius Fischer from IHFG for sharing the experimental data of 2D map.

Thanks to my family and friends, Mr. Jun Matsumoto for encouraging me during my bachelor study.